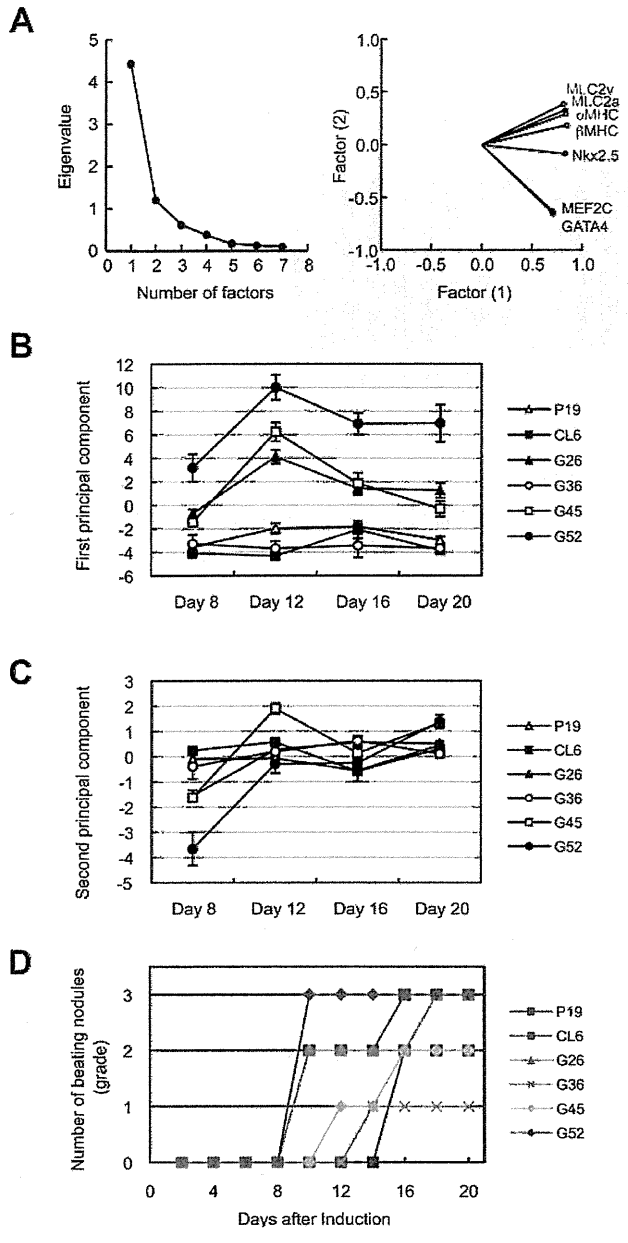

Figure S1 Cardiomyogenesis of P19 cells, P19CL6 cells and P19CL6 cell sublines

(**A–C**) PCA was performed using expression data of cardiac marker genes [*Nkx2.5*, *Gata4*, *Mef2c*, *Myh6* (α-MHC), *Myh7* (β-MHC), *Mlc2a* and *Mlc2v*] in differentiated P19 cells, P19CL6 cells and P19CL6 cell sublines (CL6G26, CL6G36, CL6G45 and CL6G52). (**A**) Scree plot indicates eigenvalues plotted against the factor numbers (left-hand panel). Factor loadings plot compares the two factor analyses (right-hand panel). (**B**) First component scores of P19 cells, P19CL6 cells and P19CL6 cell sublines at days 8, 12, 16 and 20. (**C**) Second component scores of P19 cells, P19CL6 cells and P19CL6 cell sublines at days 8, 12, 16 and 20. (**D**) P19 cells, P19CL6 cells and P19CL6 cell sublines (CL6G26, CL6G36, CL6G45 and CL6G52) were differentiated in the presence of 1 % DMSO. Nodules exhibiting spontaneous beating were counted with a microscope every other day and assessed non-parametrically, as described in the Materials and methods section of the main paper.

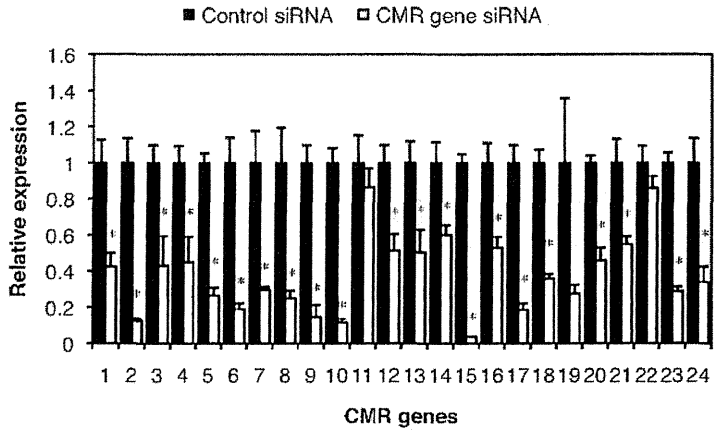

Figure S2 Efficiency of CMR gene knockdown by siRNA targeting the CMR genes in EC cells

CL6G52 cells were transfected with 100 nM siRNA targeting the CMR genes or the negative control siRNA. After 48 h, total RNA was isolated from the transfected cells. mRNA levels of the CMR genes were measured by qRT-PCR and normalized to 18S rRNA levels. Expression levels in cells transfected with the negative control were set to 1. Results are means $\pm$ S.E.M. ($n = 6$). Statistical significance was determined using a Student's t test (*$P < 0.05$ compared with control).

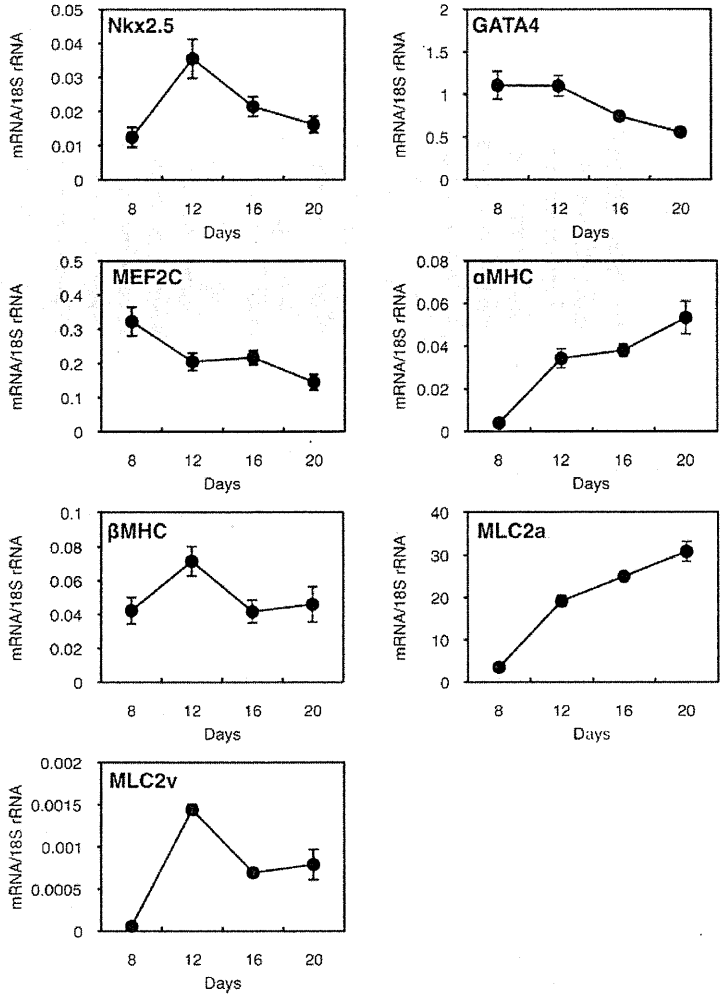

Figure S3 Transcript expression of cardiac marker genes in differentiated EC cells

An EC cell strain, CL6G52, was differentiated in the presence of 1 % DMSO. Total RNA was isolated from differentiated CL6G52 cells at days 8, 12, 16 and 20 and was subjected to one-step qRT-PCR. mRNA levels of *Nkx2.5*, *Gata4*, *Mef2c*, *Myh6* (α-MHC), *Myh7* (β-MHC), *Mlc2a* and *Mlc2v* were normalized to 18S rRNA levels. Results are means $\pm$ S.E.M. ($n = 6$).

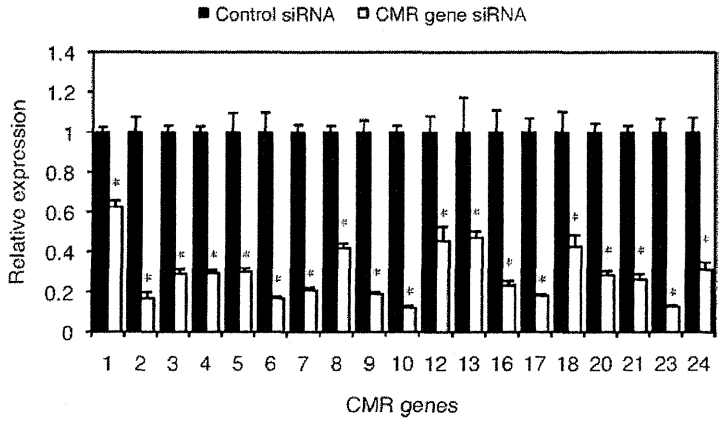

Figure S4 Efficiency of CMR gene knockdown by siRNA targeting the CMR genes in ES cells

R1 cells were transfected with 50 nM siRNA targeting the CMR genes or the negative control siRNA in the presence of 1000 units/ml LIF. After 24 h, total RNA was isolated from the transfected cells. mRNA levels of the CMR genes were measured by qRT-PCR and normalized to those of *Gapdh*. Expression levels in cells transfected with the negative control were set to 1. Results are means ± S.E.M. ($n = 5$). Statistical significance was determined using a Student's *t* test (*$P < 0.05$ compared with control).

Table S1 Probes and primers for qRT-PCR

Gene names are provided in the main paper.

Gene	Probe sequences (5′→3′)	Forward primer sequences (5′→3′)	Reverse primer sequences (5′→3′)
Nkx2.5	TGCTGAAGCTCACGTCCACGCAG	CTTCAAGCAACAGCGGTACCT	CGCTGTCGCTTGCACTTGTA
Gata4	TGCATCTCCTGTCACTCAGACATCGCA	TGCTCTAAGCTGTCCCCACAA	GTGATTATGTCCCCATGACTGTCA
Mef2c	CCAGTTACCATCCCAGTGTCCAGCCATAAC	TCCACCTCCCAGCTTTGAGAT	TGACAGGATTGCTGTACACCAAAC
Mlc2a	AAGGCCTTCAGCTGCATTGACCAGAAC	AAGCCCAGATTCAGGATTCAAG	AGCTCTTCCTCCGGAACACTT
Mlc2v	CATGGACCAGAACAGAGACGGCTTCA	GGAGTTCAAGGAAGCCTTCACA	TGTGTCCCTTAGGTCATTCTTGTC
Myh6 (α-MHC)	TCTGCTGATACCGGTGACAGTGGTAAAGG	CATGGCTACACTCTTCTCTACCTATGC	GGTGGAGAGCAGACACTGTTTG
Myh7 (β-MHC)	ACCCCTACGATTATGCGTTCATCTCCCAA	TTTCTACCAAATCCTGTCTAATAAAAAGC	GTCATCAATGGAGGCCACAGT
Nanog	ACTCCACTGGTGCTGAGCCCTTCTGA	CAGTGGTTGAAGACTAGCAATGG	GCTGCAATGGATGCTGGGA
Oct3/4	CCCGAGGAGTCCCAGGACATGAAAGC	CGTGAAGTTGGAGAAGGTGGAA	CCAAGGTGATCCTCTTCTGCTTC
T/brachyury	TGCCAGCACCAGGAACAAGCCACC	AGCAGCCGGGGTATTCCC	CTGAGGGTGGGAGCTGGC
Mesp1	AGCCCAGTCCCTCATCTCCGCTCTTC	CATCCCAGGAAAGGCAGGAAA	GCGGCGTCCAGGTTTCTAG
Tbx5	Mm00803518_m1 (Applied Biosystems)		

CMR gene	Probe sequences (5′→3′)	Forward primer sequences (5′→3′)	Reverse primer sequences (5′→3′)
Prdm5	CCACAGTGTGAATCGAGCTTTCCCAGTG	AGGTCACCTTGGCTGTGAAGA	CCGCAGTTCTCGCATTTGA
AW551984	CCGATGGACGTGAGGACAGTAATCTGGA	CCATCCTGAATCCTAGATACCATCTC	TAGTGGCAACCATGCTGAGTGT
D430028G21Rik	AGTGCACTCTTGGCTGTATTCCTGGCA	CCCCAAGAAGAGGAAGAACATTG	CGCCTACTACGGTACAGCATCA
5330410G16Rik	TCTCCCTTCGGTACCTGTTTTCCATGC	GGAGCAGAAGGACTTGGCTTT	GGAATATGTCCAGGAGGAGGATAGA
Tmem98	CCAAGATGAAGACGTCAGCAAGTGTCAGTG	CAGAAAAACTCGTTGCCATGAC	GTTTGGCCACCACAATGATG
Ctsc	TTCAACCCCTTCGAGCTGACAAATCATG	ACGATGACTTCCTACACTACCACAGT	CCATAGCCCACAAGCAAAACA
F2r	CTTTCTTGTGCCGTTGATCGTTTCCAC	CGTCCTCAGTGAGAACCTGATG	ACAAAGCCCGCGACTTCTT
Sema3e	CCGAGCACAGCAGTAAAGGTAGAAGAATGC	GTGAGTGACGGCTACAGAGAGATATACT	CACACTCATTTGCGTCTTTTCC
Maged2	AGGCTATGACAATGCCTACAACCCCGA	AGCTGACACCAAGACGCAGAA	GTACCCTCAGGCTCTGGTTCAT
2810405K02Rik	TGTCTGGTGACCTGCTGCAAAGTGGA	CCAAGGCTAAAGCTGTTGGTATC	TCTGGATGAAGTGCAACAGTACCT
Rhox4b	TGTGGGCGTGAATGGAAAGTCTA	GCCCTAATTATTCTTGTCCTTATTTGTAA	CGCAGGCTTCCTACCTTGTG
Cd302	ACCTGTGGTTTTCTGTACACCAAGAC	GATCAAGATGGTGAGGACCTAGTTG	CACAATCCCCTTTTCTCCATTC
Fzd1	ACTTCTTTCCTGCTGGCCGGTTTCGT	CGCCTCTCTTCGTTTATCTGTTC	TCTCTGTCTTGGTGCCGTCAT
Adarb1	ACCTGCCACCGCTCTACACTCTCAACAA	GTACCAGCGGATCTCCAACATAG	TGCCTCTGCATTGCTGATG
Gpaa1	CAGCGCACTTACATGTCTGAGAATGCCA	TGGCTTTTCCGCCGTTAAC	CAAACTGTTCTCTCACCATGGT
Chst2	CTTCGGTGAGCTCTTCAACCAGAAC	GACAAGCGGCAGTTGGTGTAT	CCACACAGGCTCATAGAGGAAGA
9830115L13Rik	TCCACCAGGACATTAGACAGTCGTAAAG	AGGTTGTAGGTCCCGCATACA	CCACACACAAACTGTTCGTTCTG
9630055N22Rik	CAGATGGTTTCAGAAGCTGTTGCA	CATCACCTGTGTCTGCCTTCA	GGTGGCATTCCAGTTGCTAAC
Ptprb	TGCATGCACGGTTTAGAGCAGAAGTCG	GAACAGTTCACGGCTCCACATACC	ATCCAAAGCACACAGCCAGAA
Gstz1	AGGCATTGACTATGAGATAGTGCCCA	TCGAATTGCTCTGGCGTTAA	GTTGCCCGCCATCCTTTAT
1110021L09Rik	CAGAAAGCTGGCTCACCAAGGCAACA	CTGGAAGTGTCAAGCTGCATTT	TGGCTGGTTTGCCCTTTCT
Tsga14	AAGTGACAGCTGAGGAGATCCAAAGGCTC	CAAGTCGCTTCCCTGTCAGAT	CTCCCGTGCTGTTGATGAACT
Hnrnpa1	TTCTCAGCGACCAGGTGCCCACTTAACT	GTTGTGGAACCTAAGAGAGCTGTCT	CGTAGGTGATGTTCTTCAGTGTCTTC
Adm	TACAAGCCAGCAATCAGAGCGAAGC	CTCGCTGATGAGACGACAGTTC	GGTAGCGTTTGACACGAATGTG

Table S2 Oligonucleotide sequences for siRNAs targeting CMR genes

Gene names are provided in the main paper.

CMR gene number	Target gene	Sense sequences (5′→3′)	Antisense sequences (5′→3′)
1	*Prdm5*	GGGACAGUUGGCAGCUGGAAGUAAA	UUUACUUCCAGCUGCCAACUGUCCC
2	*AW551984*	CCGGUGAAGUGUGUCUCUCAUAUAA	UUAUAUGAGAGACACACUUCACCGG
3	*D430028G21Rik*	GCUGAGGACAAGACCUAUAAGUAUA	UAUACUUAUAGGUCUUGUCCUCAGC
4	*5330410G16Rik*	CCGGGCUGCCUCGAUGGGUCCUAUU	AAUAGGACCCAUCGAGGCAGCCCGG
5	*Tmem98*	CCACUGCAUCGCCAUCUUGAAGAUU	AAUCUUCAAGAUGGCGAUGCAGUGG
6	*Ctsc*	CCAAGGCUUCGAGAUUGUGUUGAAU	AUUCAACACAAUCUCGAAGCCUUGG
7	*F2r*	GGUAGGGCAGUCUACUUAAAUAUAA	UUAUAUUUAAGUAGACUGCCCUACC
8	*Sema3e*	CCAUACAAUGCUGCUGGAUGAGUAU	AUACUCAUCCAGCAGCAUUGUAUGG
9	*Maged2*	GGUACCGAUCCAAAGGUCAAUACAA	UUGUAUUGACCUUUGGAUCGGUACC
10	*2810405K02Rik*	GCCUCCAAGGCUAAAGCUGUUGGUA	UACCAACAGCUUUAGCCUUGGAGGC
11	*Rhox4b*	AAGCGGACGCCGTGGTCAAGA	UCUUGACCACGGCGUCCGCUU
12	*Cd302*	GGCAGACAUGGUAAGCAUACACAAU	AUUGUGUAUGCUUACGCAUGUCUGCC
13	*Fzd1*	CCAAGGUUUACGGGCUCAUGUACUU	AAGUACAUGAGCCCGUAAACCUUGG
14	*Adarb1*	GGGACGAAGUGUAUCAACGGUGAAU	AUUCACCGUUGAUACACUUCGUCCC
15	*Gpaa1*	CCCAGCGCACUUACAUGUCUGAGAA	UUCUCAGACAUGUAAGUGCGCUGGG
16	*Chst2*	GGUGAGUCCCGAAAUGGAGCAGUUU	AAACUGCUCCAUUUCGGGACUCACC
17	*9830115L13Rik*	CCCUUGCUCCGUUACCUAACGACUU	AAGUCGUUAGGUAACGGAGCAAGGG
18	*9630055N22Rik*	CCUUGAAAUACUAGCUGCUGUCUUU	AAAGACAGCAGCUAGUAUUUCAAGG
19	*Ptprb*	GCAACUGAACCUGUUAUGUUCUAUA	UAUAGAACAUAACAGGUUCAGUUGC
20	*Gstz1*	GGGAAGCCUAUCCUCUACUCCUAUU	AAUAGGAGUAGAGGAUAGGCUUCCC
21	*1110021L09Rik*	CCCAGUCCAGAGCAUUUCUUGGCUU	AAGCCAAGAAAUGCUCUGGACUGGG
22	*Tsga14*	CCCAUUGCAACUCUAUCCAGGACAA	UUGUCCUGGAUAGAGUUGCAAUGGG
23	*Hnrnpa1*	GGAACACUAACAGACUGUGUGGUAA	UUACCACACAGUCUGUUAGUGUUCC
24	*Adm*	GCUGGUUUCCAUCACCCUGAUGUUA	UAACAUCAGGGUGAUGGAAACCAGC

Table S3 Correlation of GeneChip probe set intensities with the first and second principal components, lag time to the onset of beating and number of nodules

rs, Spearman's rank correlation coefficient.

	First principal component		Second principal component		Lag time to the onset of beating		Number of nodules	
CMR gene number	rs	*P* value	rs	*P* value	rs	*P* value	rs	*P* value
CMR1	0.8237	2.26×10^{-8}	0.7368	3.44×10^{-6}	−0.4932	5.61×10^{-3}	0.4384	1.54×10^{-2}
CMR2	0.7836	3.04×10^{-7}	0.7464	2.18×10^{-6}	−0.5419	1.98×10^{-3}	0.4153	2.25×10^{-2}
CMR3	0.7596	1.13×10^{-6}	0.4397	1.51×10^{-2}	−0.6333	1.73×10^{-4}	0.6455	1.17×10^{-4}
CMR4	0.7596	1.13×10^{-6}	0.6386	1.46×10^{-4}	−0.4859	6.48×10^{-3}	0.4202	2.08×10^{-2}
CMR5	0.7573	1.27×10^{-6}	0.466	9.44×10^{-3}	−0.6856	2.90×10^{-5}	0.6881	2.64×10^{-5}
CMR6	−0.7196	7.42×10^{-6}	−0.5235	2.99×10^{-3}	0.6771	3.97×10^{-5}	−0.5907	5.90×10^{-4}
CMR7	0.6589	7.52×10^{-5}	0.1282	5.00×10^{-1}	−0.492	5.75×10^{-3}	0.6004	4.52×10^{-4}
CMR2	0.6521	9.46×10^{-5}	0.3798	3.85×10^{-2}	−0.8038	8.85×10^{-8}	0.7672	7.57×10^{-7}
CMR8	−0.6246	2.25×10^{-4}	−0.4588	1.08×10^{-2}	0.4177	2.16×10^{-2}	−0.3824	3.70×10^{-2}
CMR9	−0.5903	5.96×10^{-4}	−0.3103	9.52×10^{-2}	0.503	4.61×10^{-3}	−0.5164	3.49×10^{-3}
CMR10	0.5658	1.12×10^{-3}	0.2336	2.14×10^{-1}	−0.6151	2.98×10^{-4}	0.6455	1.17×10^{-4}
CMR11	0.5651	1.14×10^{-3}	0.4277	1.84×10^{-2}	−0.6308	1.86×10^{-4}	0.5858	6.71×10^{-4}
CMR12	0.556	1.42×10^{-3}	0.4157	2.23×10^{-2}	−0.3982	2.93×10^{-2}	0.4165	2.21×10^{-2}
CMR13	0.5399	2.07×10^{-3}	0.3055	1.01×10^{-1}	−0.4299	1.77×10^{-2}	0.4323	1.70×10^{-2}
CMR13	0.5388	2.13×10^{-3}	0.1761	3.52×10^{-1}	−0.5858	6.71×10^{-4}	0.682	3.32×10^{-5}
CMR14	0.5366	2.24×10^{-3}	0.2432	1.95×10^{-1}	−0.4671	9.26×10^{-3}	0.5012	4.78×10^{-3}
CMR15	0.485	6.59×10^{-3}	0.0012	9.95×10^{-1}	−0.6735	4.53×10^{-5}	0.7806	3.61×10^{-7}
CMR16	0.4685	9.02×10^{-3}	−0.1186	5.32×10^{-1}	−0.4744	8.08×10^{-3}	0.64	1.40×10^{-4}
CMR17	−0.4559	1.13×10^{-2}	−0.0503	7.92×10^{-1}	0.7673	7.53×10^{-7}	−0.8313	1.28×10^{-8}
CMR18	0.453	1.19×10^{-2}	−0.0635	7.39×10^{-1}	−0.369	4.48×10^{-2}	0.548	1.72×10^{-3}
CMR19	−0.4404	1.49×10^{-2}	−0.1066	5.75×10^{-1}	0.643	1.27×10^{-4}	−0.7124	1.00×10^{-5}
CMR20	−0.4256	1.91×10^{-2}	0.0036	9.85×10^{-1}	0.4214	2.04×10^{-2}	−0.5395	2.09×10^{-3}
CMR21	0.397	2.99×10^{-2}	−0.0204	9.15×10^{-1}	−0.5809	7.63×10^{-4}	0.6832	3.17×10^{-5}
CMR22	−0.3924	3.20×10^{-2}	−0.2839	1.28×10^{-1}	0.5249	2.90×10^{-3}	−0.4579	1.09×10^{-2}
CMR23	−0.3924	3.20×10^{-2}	0.109	5.66×10^{-1}	0.6978	1.81×10^{-5}	−0.822	2.54×10^{-8}
CMR24	−0.3856	3.53×10^{-2}	0.1414	4.56×10^{-1}	0.4623	1.01×10^{-2}	−0.603	4.20×10^{-4}

Table S4 Effects of CMR gene knockdown on cardiac marker gene expression and the number of nodules in differentiated EC cells and ES cells

*Not significant (NS; $P \geqslant 0.05$); †transcript expression significantly decreased compared with the control ($P < 0.05$); ‡transcript expression significantly increased compared with the control ($P < 0.05$).

	Myh6 (α-MHC)		*Myh7* (β-MHC)		*Mlc2a*		*Mlc2v*		
Gene targeted	EC cells	ES cells	EC cells	ES cells	EC cells	ES cells	EC cells	ES cells	Number of nodules (EC cells)
CMR1	NS*	NS	NS	NS	NS	NS	NS	NS	NS
CMR2	Down†	Down	Down	Down	Down	Down	Down	Down	Down
CMR3	Down	NS	NS	NS	NS	NS	Down	NS	Down
CMR4	Down	NS	NS	NS	Down	NS	Down	NS	Down
CNR5	Down	NS	NS	NS	NS	NS	Down	NS	Down
CMR6	NS	NS	NS	NS	NS	NS	Down	NS	NS
CMR7	NS	NS	NS	Up‡	NS	Up	Up	NS	Up
CMR8	NS	Down	NS	Down	Down	Down	NS	NS	NS
CMR9	NS	NS	NS	Up	NS	Up	NS	Up	Down
CMR10	Down	Down	NS	Down	Down	Down	Down	Down	Down
CMR12	Up	Up	NS	Up	NS	Up	Up	NS	Up
CMR13	Down	NS	Down	NS	NS	NS	Down	NS	Down
CMR14	NS	Down	NS	Down	NS	Down	NS	Down	NS
CMR15	NS	Down	NS	Down	NS	Down	NS	Down	NS
CMR16	NS	NS	Up	NS	Up	NS	Up	NS	Up
CMR17	NS	NS	Up	NS	NS	NS	NS	NS	Up
CMR18	Down	NS	NS	NS	NS	NS	NS	NS	Down
CMR20	NS	Down	NS	NS	Down	Down	NS	NS	NS
CMR21	NS	NS	NS	Up	NS	Up	NS	NS	Up
CMR23	Up	Down	Up	Down	Down	Down	Up	Down	Up
CMR24	NS	NS	NS	Up	NS	Up	NS	NS	Down

Received 22 March 2011/3 May 2011; accepted 10 May 2011
Published as BJ Immediate Publication 10 May 2011, doi:10.1042/BJ20110520

Biochemical and Biophysical Research Communications 409 (2011) 108–113

Contents lists available at ScienceDirect

Biochemical and Biophysical Research Communications

journal homepage: www.elsevier.com/locate/ybbrc

TRPC3-mediated Ca^{2+} influx contributes to Rac1-mediated production of reactive oxygen species in MLP-deficient mouse hearts

Naoyuki Kitajima [a], Kunihiro Watanabe [a], Sachio Morimoto [b], Yoji Sato [c], Shigeki Kiyonaka [d], Masahiko Hoshijima [e], Yasuhiro Ikeda [f], Michio Nakaya [a], Tomomi Ide [g], Yasuo Mori [d], Hitoshi Kurose [a], Motohiro Nishida [a,*]

[a] Department of Pharmacology and Toxicology, Graduate School of Pharmaceutical Sciences, Kyushu University, Fukuoka 812-8582, Japan
[b] Department of Clinical Pharmacology, Graduate School of Medical Sciences, Kyushu University, Fukuoka 812-8582, Japan
[c] Division of Cellular and Gene Therapy Products, National Institute of Health Sciences, Tokyo 158-8501, Japan
[d] Laboratory of Molecular Biology, Department of Synthetic Chemistry and Biological Chemistry, Graduate School of Engineering, Kyoto University, Kyoto 615-8510, Japan
[e] Department of Medicine, Division of Cardiology, University of California San Diego, La Jolla, CA 92093-0734, USA
[f] Division of Cardiology, Department of Medicine and Clinical Science, Yamaguchi University Graduate School of Medicine, Yamaguchi 755-8505, Japan
[g] Department of Cardiovascular Medicine, Graduate School of Medical Sciences, Kyushu University, Fukuoka 812-8582, Japan

ARTICLE INFO

Article history:
Received 19 April 2011
Available online 3 May 2011

Keywords:
Transient receptor potential channel
Muscle LIM protein
Dilated cardiomyopathy
Rac
Reactive oxygen species

ABSTRACT

Dilated cardiomyopathy (DCM) is a myocardial disorder that is characterized by dilation and dysfunction of the left ventricle (LV). Accumulating evidence has implicated aberrant Ca^{2+} signaling and oxidative stress in the progression of DCM, but the molecular details are unknown. In the present study, we report that inhibition of the transient receptor potential canonical 3 (TRPC3) channels partially prevents LV dilation and dysfunction in muscle LIM protein-deficient (MLP (−/−)) mice, a murine model of DCM. The expression level of TRPC3 and the activity of Ca^{2+}/calmodulin-dependent kinase II (CaMKII) were increased in MLP (−/−) mouse hearts. Acitivity of Rac1, a small GTP-binding protein that participates in NADPH oxidase (Nox) activation, and the production of reactive oxygen species (ROS) were also increased in MLP (−/−) mouse hearts. Treatment with pyrazole-3, a TRPC3 selective inhibitor, strongly suppressed the increased activities of CaMKII and Rac1, as well as ROS production. In contrast, activation of TRPC3 by 1-oleoyl-2-acetyl-*sn*-glycerol (OAG), or by mechanical stretch, induced ROS production in rat neonatal cardiomyocytes. These results suggest that up-regulation of TRPC3 is responsible for the increase in CaMKII activity and the Nox-mediated ROS production in MLP (−/−) mouse cardiomyocytes, and that inhibition of TRPC3 is an effective therapeutic strategy to prevent the progression of DCM.

1. Introduction

Dilated cardiomyopathy (DCM), a poorly understood disorder in which the LV chambers enlarge, is the most common causes for congestive heart failure [1]. Heart failure resulting from DCM is a principal cause of death and disability in children and young adults. Despite recent progress in the treatment of heart failure, the only meaningful treatment for DCM is cardiac transplantation. Although most cases of DCM develop as a consequence of specific inflammatory, metabolic or toxic insults [2], 25–35% of DCM cases are caused by genetic mutations [3–5]. Affected genes encode proteins that function in the Ca^{2+} regulatory system, the contractile/cytoskeltal apparatus, or reside at a sarcomeric Z-disk. One of the Z-disk proteins that has been implicated in DCM etiology is the muscle LIM protein (MLP) [6–8]. MLP interacts with telethonin, a titin-interacting protein, to form a component of the mechanical stretch apparatus [8], and genetic ablation of MLP in mice causes age-related DCM, which closely resembles human DCM [8,9]. Thus, MLP deficient (MLP (−/−)) mice are commonly employed as a murine DCM model system. Since genetic ablation of angiotensin (Ang) II type1 receptor (AT_1R) or overexpression of the carboxyl-terminal region of the β adrenergic receptor (βAR) kinase (βARK-ct) attenuates the

Abbreviations: Ang, angiotensin; AT_1R, Ang type1 receptor; βAR, β adrenergic receptor; βARK, βAR kinase; βARK-ct, carboxyl-terminal region of βARK (βARK inhibitor); CaMKII, Ca^{2+}/calmodulin-dependent kinase II; DAG, diacylglycerol; DCF, dichlorofluorescein; DCM, dilated cardiomyopathy; DHE, dihydroethidium; DPI, diphenyleneiodonium; 4-HNE, 4-hydroxy-2-nonenal; LV, left ventricle; MLP, muscle LIM protein; LTCCs, L-type Ca^{2+} channels; NFAT, nuclear factor of activated T cells; Nox, NADPH oxidase; OAG, 1-oleoyl-2-acetyl-*sn*-glycerol; PKC, protein kinase C; pyrazole-3 (Pyr3), ethyl-1-(4-(2*3*3-trichloroacrylamide)phenyl)-5-(trifluoromethyl)-1H-pyrazole-4-carboxylate; ROS, reactive oxygen species; RIRR, ROS-induced ROS release; TRP, transient receptor potential; TRPC, TRP canonical.

* Corresponding author. Address: Department of Pharmacology and Toxicology, Graduate School of Pharmaceutical, Sciences, Kyushu University, 3-1-1 Maidashi, Higashi-ku, Fukuoka, Fukuoka 812-8582, Japan. Fax: +81 92 642 6878.
E-mail address: nishida@phar.kyushu-u.ac.jp (M. Nishida).

0006-291X/$ - see front matter © 2011 Elsevier Inc. All rights reserved.
doi:10.1016/j.bbrc.2011.04.124

progression of heart failure in MLP (−/−) mice [10,11], βAR and AT_1R signalings are thought to participate in the progression of heart failure in MLP (−/−) mice.

Abnormal Ca^{2+} metabolism and production of ROS have been implicated in the progressive deterioration of heart failure [12–14]. For example, activation of CaMKIIδ causes p53 accumulation and cardiomyocyte apoptosis in DCM [13]. In contrast, $p47^{phox}$, a Nox subunit, and the small GTP-binding protein Rac1, are up-regulated and oxygen free radical release is increased in human LV myocardium from patients with DCM [14]. Furthermore, oxidative stress inactivates calcineurin, a Ca^{2+}-dependent protein phosphatase that mediates cardiac hypertrophy, indicating the functional cross-talk between Ca^{2+} signaling and ROS signaling [12]. Although both Ca^{2+} and ROS evidently play key roles in the progression of heart failure, their upstream regulator(s) remain elusive.

Transient receptor potential (TRP) family proteins, first described in a *Drosophila* visual transduction mutation *trp*, comprise 28 mammalian cation channels expressed in almost every tissue [15–17]. Among them, canonical TRP subfamily (TRPC) proteins have been up-regulated in hypertrophied and failing hearts [17–20]. TRPC channels were originally proposed as store-operated channels activated by Ca^{2+} depletion of stores, while closely related TRPC3, TRPC6, and TRPC7 showed activation sensitivity to the membrane-delimited action of diacylglycerol (DAG). In particular, TRPC1, TRPC3 and TRPC6 proteins participate in agonist-induced cardiomyocyte hypertrophy through activation of Ca^{2+}-dependent calcineurin/nuclear factor of activated T cells (NFAT) signaling pathways [18–20]. We have reported that TRPC3 and TRPC6 channels mediate the Ang II-induced cardiomyocyte hypertrophy *in vitro* and pressure overload-induced cardiac hypertrophy *in vivo* [21,22]. The TRPC3/6-mediated cation influx induces membrane depolarization, followed by an increase in the frequency of Ca^{2+} transients evoked by voltage-dependent Ca^{2+} influx-induced Ca^{2+} release, leading to NFAT activation in rat cardiomyocytes [21]. However, calcineurin/NFAT signaling is apparently desensitized in MLP (−/−) mouse hearts, as MLP is essential for mechanical stretch-induced NFAT activation through anchorage of calcineurin at the Z-disk [23]. Therefore, it is unknown whether TRPC-mediated Ca^{2+} signals are involved in the progression of heart failure in MLP (−/−) mice.

In the present study, we examine the effects of a selective TRPC3 inhibitor, pyrazole-3 (Pyr3) [22], in the progression of DCM using the MLP (−/−) mouse model. We demonstrate that TRPC3-mediated Ca^{2+} signals are increased in MLP (−/−) mouse hearts, and Pyr3 potently inhibits LV dysfunction, CaMKII activation and ROS production. The inhibitory effect of Pyr3 on LV dysfunction is apparently small compared to the pronounced effects on CaMKII activation and ROS production, indicating that TRPC3 only plays a complementary role in the progression of DCM. However, our findings suggest that TRPC3 blockade is a therapeutic strategy for preventing DCM.

2. Materials and methods

2.1. Animals and drug treatment

The basal cardiomyopathic phenotype of MLP (−/−) mice was described previously [7,8]. Wild type littermates (MLP (+/+)) served as controls for all studies. A mini osmotic pump (Alzet) filled with pyrazole 3 (Pyr3), a selective inhibitor of TRPC3, or polyethylene glycol 300 (vehicle) was implanted intraperitoneally into 5-week-old mice, and Pyr3 (0.1 mg/kg/day) was continuously administered for 3 weeks. All animal care procedure and experiments were approved by the guidelines of Kyushu University.

2.2. Transthoracic echocardiography and cardiac catheterization

Echocardiography was performed in anesthetized mice (50 mg/kg pentobarbital sodium) by using Nemio-XG echocardiograph (TOSHIBA) equipped with a 14 MHz transducer. A 1.4 French micronanometer catheter (Millar Instruments, Houston, TX) was inserted into the left carotid and advanced retrograde into the LV. Hemodynamic measurements were recorded when heart rate was stabilized within 500 ± 10 beats/min.

2.3. Histological analysis of mouse hearts

The paraffin-embedded LV sections (5 μm in thickness) were stained with hematoxylin and eosin (H&E) or picrosirius red, and cell-sectional area (CSA) of cardiomyocytes and collagen volume fraction (CVF) of LV sections were analyzed using BZ-II analyzer (Keyence) [24].

2.4. Isolation of cardiomyocytes and siRNA treatment

Rat neonatal cardiomyocytes were prepared as described previously [25]. For knockdown of rat TRPC3 proteins, cells were transfected with siRNA (100 nM) for TRPC3 using lipofectamine2000 for 72 h [26]. Adult mouse cardiomyocytes were isolated from 8-week-old mouse hearts as described previously [5].

2.5. Real time PCR, pulldown assay, and Western blot analysis

RNA extraction, real time RT-PCR and Rac pulldown assay were performed as described previously [24]. Hearts were homogenized in RIPA buffer (pH 8.0) containing 0.1% SDS, 0.5% sodium deoxycholate, 1% NP-40, 150 mM NaCl, 50 mM Tris–HCl, and protease inhibitor cocktail (Nacalai). Supernatants (10 μg) were fractionated by SDS–PAGE gel, and expression levels of endogenous proteins were detected by antibodies raised against ACE (1/10,000, R&D systems), Periostin (1/10,000, R&D systems), Rac1 (1/1000, BD Bioscience), CaMKII (1/1000, Santa Cruz), phospho-CaMKII (Thr286) (1/1000, Cell Signaling) and GAPDH (1/3000, Santa Cruz). Membrane fractions (10 μg) were isolated using Proteoextract transmembrane protein extraction kit (Novagen) to detect TRPC1, TRPC3, TRPC5, TRPC6 and TRPC7 proteins using respective TRPC antibodies (1/2000, Alomone). Proteins were visualized with chemiluminescent detection of antibodies conjugated with horseradish peroxidase (ECL plus, Perkin Elmer). The optical density of the film was scanned and measured with Scion Image Software.

2.6. Measurement of ROS production and intracellular Ca^{2+} concentration

The paraffin-embedded LV sections were stained with anti-4-hydroxy-2-nonenal (4-HNE) antibody (1/500: JaICA, Nikken Seil Co., Ltd.). The 4-HNE adducts were visualized with Alexa Fluor 546 anti-mouse IgG antibody (1/1000, Molecular Probes). Superoxide production in the heart was measured using dihydroethidium (DHE) [27]. Hearts were solidified with liquid nitrogen and sectioned in 10 μm thickness using Cryostat (Leica, CM1100). The LV sections were incubated with DHE (100 μM) at room temperature for 5 min. After washing the LV sections with PBS, digital photographs were taken at ×60 magnification using confocal microscopy (FV10i, Olympus), and 5 regions selected at random for each specimen of the heart. The average intensity was analyzed using MetaMorph Software. Measurement of intracellular Ca^{2+} concentration ($[Ca^{2+}]_i$) in adult mouse cardiomyocytes was performed using fura-2 [26]. Production of ROS in rat neonatal cardiomyocytes was measured using 2′,7′-dichlorofluorescein diacetate ($DCFH_2DA$) and DHE [27]. Cells plated on laminin-coated silicone rubber

culture dishes were loaded with $DCFH_2DA$ (10 μM) at 37 °C for 10 min. The DCF fluorescence or fura-2 fluorescence at an emission wavelength of 510 nm was observed at room temperature by exciting DCF at 488 nm or exciting fura-2 at 340 nm and 380 nm using a video image analysis system (Aquacosmos, Hamamatsu Photonics).

2.7. Statistical analysis

The results are shown as means ± S.E.M. All experiments were repeated at least three times. Statistical comparisons were made with two-tailed Student's *t*-test or one way analysis of variance followed by the Student–Newman–Keuls procedure with significance imparted at $P < 0.05$.

3. Results

3.1. Increase in TRPC3-mediated Ca^{2+} signals in MLP (−/−) mouse hearts

Compared with MLP (+/+) mouse hearts, the expression levels of TRPC3 and TRPC6 proteins, but not TRPC1, TRPC5, and TRPC7, were significantly increased in MLP (−/−) mouse hearts (Fig. 1A). Treatment of isolated MLP (+/+) mouse cardiomyocytes with OAG induced a Ca^{2+} influx-mediated increase in $[Ca^{2+}]_i$. This $[Ca^{2+}]_i$ increase was completely suppressed by the addition of Pyr3 (Fig. 1B). The OAG-induced maximal $[Ca^{2+}]_i$ increase was markedly enhanced in MLP (−/−) mouse cardiomyocytes (Fig. 1C), indicating that up-regulation of TRPC3 enhances DAG-mediated Ca^{2+} influx. NFAT and CaMKII are two major downstream effectors of Ca^{2+}/calmodulin-mediated cardiac hypertrophy [17]. The CaMKII activity was increased in MLP (−/−) mouse hearts (Fig. 1D). This CaMKII activation was significantly suppressed by Pyr3 treatment. These results suggest that up-regulation of TRPC3 contributes to Ca^{2+} influx-dependent CaMKII activation in MLP (−/−) mouse hearts.

3.2. Inhibition of TRPC3 attenuates LV dilation and dysfunction

Both LV wall thickness and LV function were markedly reduced in 8-week-old MLP (−/−) mouse hearts (Tables 1 and 2). Treatment of MLP (−/−) mice with Pyr3 significantly attenuated the progression of LV dilation and dysfunction. Inhibition of TRPC3 also reduced the increase in heart weight and cardiomyocyte hypertrophy (Fig. 2A–C) and the increases in mRNAs of hypertrophy-related markers (β-myosin heavy chain (βMHC), α-skeletal muscle actin (αSKA) and Ang converting enzyme (ACE)) (Fig. 2D). We previously reported that cardiac hypertrophy and fibrosis are independently regulated by two heterotrimeric GTP-binding proteins [24]. Therefore, we next examined whether inhibition of TRPC3 suppresses cardiac fibrosis in MLP (−/−) mice. Collagen deposition in the interstitial area was markedly increased in MLP (−/−) hearts, and this fibrosis was suppressed by Pyr3 treatment (Fig. 3A and B). Pyr3 also suppressed the increase in expression of fibrosis-inducible proteins (ACE and periostin) in MLP (−/−) mouse hearts (Fig. 3C). These results suggest that inhibition of TRPC3 attenuates the development of cardiac hypertrophy and fibrosis in MLP (−/−) mice.

3.3. TRPC3-mediated Ca^{2+} influx contributes to ROS production

It is generally thought that oxygen free radical release is increased in the failing heart and oxidative stress is a major cause of the progression of heart failure [12,14]. Up-regulation of TRPC3 channels participate in CaMKII activation in MLP (−/−) mouse hearts, and it has been reported that Ca^{2+} influx is required for Nox-mediated ROS production [28,29]. Therefore, we examined whether TRPC3-mediated Ca^{2+} influx regulates ROS production in DCM. The expression level of 4-HNE adducts and superoxide production were markedly increased in MLP (−/−) mouse hearts (Fig. 4A and B). These ROS accumulations

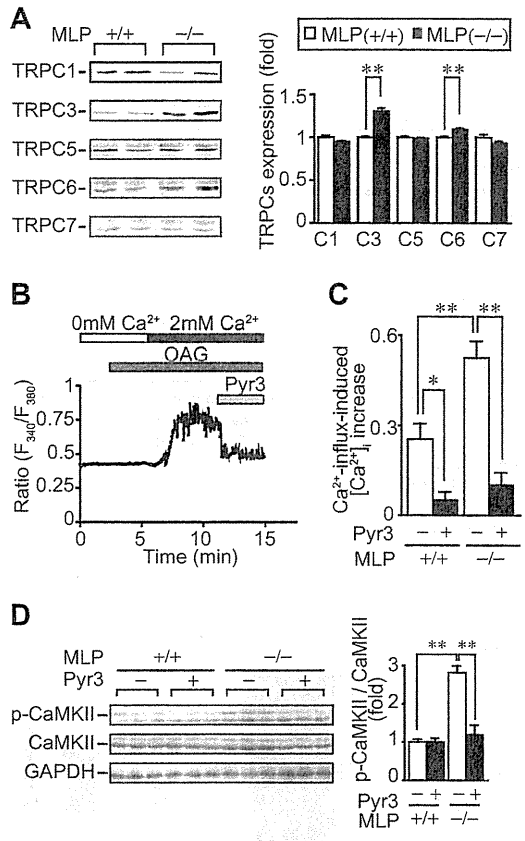

Fig. 1. Involvement of TRPC3 in CaMKII activation of MLP-deficient hearts. (A) Protein expression levels of respective TRPC channels in wild type (MLP (+/+)) and MLP-deficient (MLP (−/−)) mouse hearts. Hearts were removed from 5 week-old mice. ($n = 4$) $^{**}P < 0.01$ (B) Typical time course of Ca^{2+} response induced by OAG (15 μM) in the absence (0 mM Ca^{2+}) or presence of extracellular Ca^{2+} (2 mM Ca^{2+}) in isolated MLP (+/+) mouse cardiomyocytes. Cells were treated with Pyr3 (1 μM). ($n = 10$–12) (C) Maximal Ca^{2+} influx-mediated increase in $[Ca^{2+}]_i$ induced by OAG. (D) Effects of pyrazole-3 (Pyr3) on the phosphorylation of CaMKII proteins. ($n = 6$) $^{*}P < 0.05$.

Table 1
Echocardiographic parameters.

	MLP(+/+) Veh ($n = 5$)	MLP(+/+) Pyr3 ($n = 5$)	MLP(−/−) Veh ($n = 11$)	MLP(−/−) Pyr3 ($n = 11$)
HR (bpm)	538 ± 10	541 ± 14	533 ± 11	529 ± 16
IVSd (mm)	0.88 ± 0.04	0.90 ± 0.03	0.63 ± 0.03**	0.92 ± 0.04$^{\#\#}$
LVPWd (mm)	0.98 ± 0.02	0.94 ± 0.02	0.71 ± 0.04**	0.97 ± 0.04$^{\#\#}$
LVIDd (mm)	2.08 ± 0.09	2.04 ± 0.02	3.25 ± 0.17**	2.64 ± 0.04$^{\#\#}$
LVIDs (mm)	0.50 ± 0.06	0.48 ± 0.02	2.48 ± 0.19**	1.39 ± 0.18$^{\#\#}$
EF (%)	98.8 ± 0.3	98.8 ± 0.2	56.0 ± 3.9**	83.2 ± 3.4$^{\#\#}$
FS (%)	78.0 ± 2.1	78.0 ± 1.1	25.4 ± 1.1**	50.6 ± 4.7$^{\#\#}$

HR, heart rate; IVSd, interventricular septum diastolic diameter; LVPWd, left ventricular posterior wall diastolic diameter; LVIDd, left ventricular internal at end-diastole; LVIDs, left ventricular internal diameters at end-systole; EF, ejection fraction; FS, Fractional shortening; Veh, vehicle.
** $P < 0.01$ vs. MLP(+/+) Veh.
$^{\#\#}$ $P < 0.01$ vs. MLP(−/−) Veh.

Table 2
Cardiac parameters measured by Millar Catheter.

	MLP(+/+) Veh ($n = 5$)	MLP(+/+) Pyr3 ($n = 5$)	MLP(−/−) Veh ($n = 11$)	MLP(−/−) Pyr3 ($n = 11$)
Heart Rate (bpm)	498 ± 3	504 ± 2	500 ± 4	505 ± 1
LVESP (mm Hg)	123 ± 4	127 ± 3	102 ± 2**	108 ± 2#
LVEDP (mm Hg)	4.4 ± 0.8	3.6 ± 1.0	14.1 ± 1.2**	8.4 ± 0.4##
dP/dt max (mm Hg/s)	13,365 ± 199	12,756 ± 412	6252 ± 294**	8235 ± 316##
dP/dt min (mm Hg/s)	8049 ± 617	8444 ± 530	3240 ± 185**	4516 ± 178##
Tau (msec)	9.8 ± 0.4	8.9 ± 0.2	28.7 ± 1.8**	20.2 ± 0.8##

HR, heart rate; LVESP, left ventricular end systolic pressure; LVEDP, left ventricular end diastolic pressure; dP/dt max, maximal rate of pressure development; dP/dt min, maximal rate of decay of pressure; Tau, monoexponential time constant of relaxation. Veh, vehicle.
** $P < 0.01$ vs. MLP(+/+) Veh.
# $P < 0.05$.
$P < 0.01$ vs. MLP(−/−) Veh.

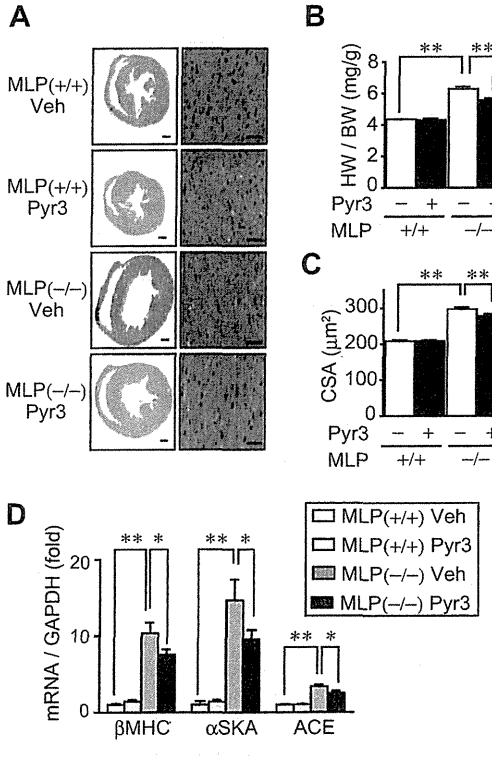

Fig. 2. Inhibition of TRPC3 attenuates left ventricular dysfunction in MLP-deficient mice. Effects of Pyr3 on morphological changes (A)–(C) and hypertrophic gene expression (D) in MLP (+/+) and MLP (−/−) mouse hearts. (A) H&E-stained mid-transverse LV sections of the hearts isolated from 8 week-old mice. Bars = 400 μm (left) and 50 μm (right). ($n = 5$–11) (B) Heart weight (HW) to body weight (BW) ratios. (C) Average areas of cardiomyocytes. ($n = 5$). (D) Expressions of β-MHC, α-SKA and ACE mRNAs. ($n = 4$) *$P < 0.05$, ** $P < 0.01$.

were completely suppressed by Pyr3. Mitochondria and Nox are two major sources of ROS in the heart. The heart expresses two Nox isoforms: Nox2 and Nox4 [30,31], and up-regulation of either isoform has been reported to induce mitochondrial

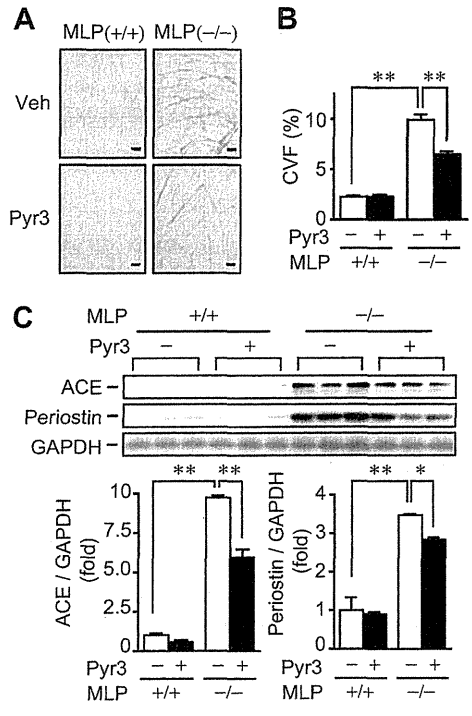

Fig. 3. Inhibition TRPC3 attenuates interstitial fibrosis of MLP-deficient mice. (A) LV sections stained by picrosirius red (Bars = 50 μm). (B) Results of fibrosis in MLP (−/−) and MLP (+/+) mouse hearts with or without Pyr3. ($n = 5$) (C) Effects of Pyr3 on the expressions of ACE, periostin, and GAPDH proteins. ($n = 6$) *$P < 0.05$, **$P < 0.01$.

dysfunction in the heart [14,31]. The Nox2 activity is predominantly regulated by Rac, $p47^{phox}$, $p67^{phox}$, and $p22^{phox}$, while Nox4 is constitutively activated [32]. In addition, Rac1 has been implicated in the progression of DCM [14]. Although Nox2 and Nox4 mRNA levels were not increased in MLP (−/−) mouse hearts (data not shown), the expression and activity of Rac1 were markedly increased (Fig. 4C). Treatment with Pyr3 significantly suppressed Rac1 activation without affecting total Rac1 protein levels. These results suggest that up-regulation of TRPC3 contributes to Rac1-mediated ROS production in MLP (−/−) mouse hearts. We further examined whether activation of TRPC3 actually induces ROS production in rat neonatal cardiomyocytes. We recently reported that mechanical stretch induces a Ca^{2+} response through activation of TRPC3/6 channels [26]. Mechanical stretch of cardiomyocytes gradually increased DCF fluorescence intensity (Fig. 4D). This ROS production was significantly suppressed by Pyr3 or knockdown of TRPC3. Treatment with OAG also induced superoxide production, and the DHE accumulation was reduced by TRPC3 knockdown or by pretreatment with Pyr3 or diphenyleneiodonium (DPI), a Nox inhibitor (Fig. 4E and F). Furthermore, the OAG-induced superoxide production was inhibited by the elimination of extracellular Ca^{2+}. These results suggest that TRPC3-mediated Ca^{2+} influx mediates ROS production through Nox activation in rodent cardiomyocytes.

4. Discussion

Several reports have suggested the involvement of TRPC up-regulation in the development of cardiac hypertrophy *in vivo* [17–20]. On the other hand, DCM is believed to represent a maladaptive response of the heart in a late stage of heart failure. We first demonstrated that TRPC3 channels participate in the

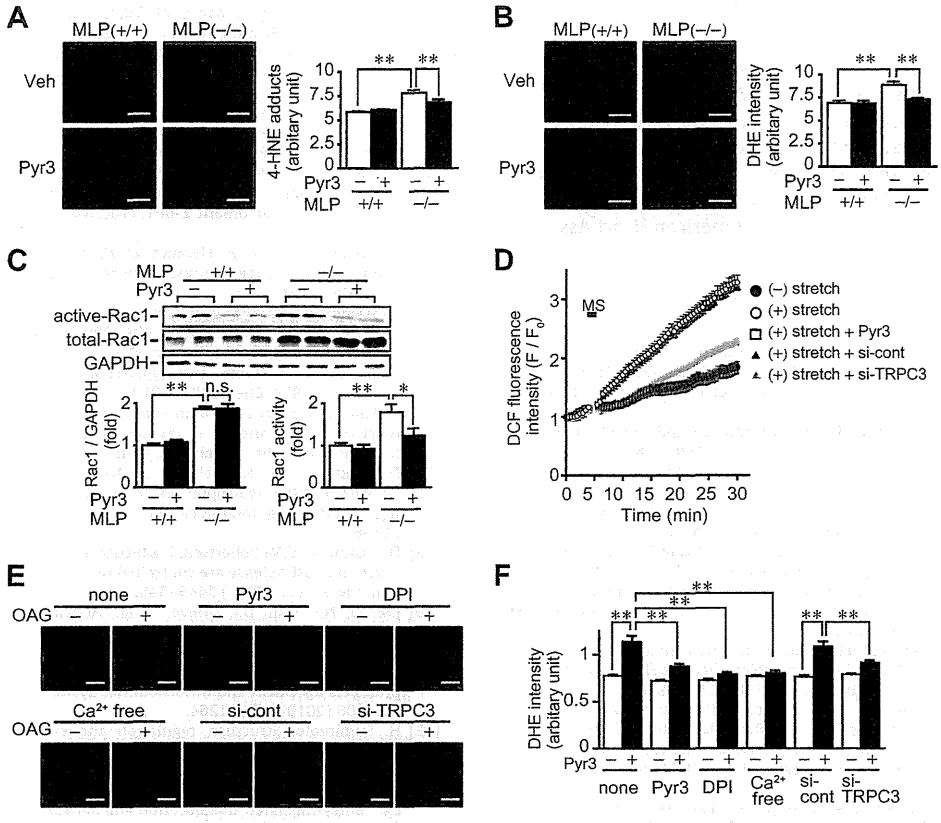

Fig. 4. TRPC3 mediates mechanical stretch-induced superoxide production in cardiomyocytes. (A) Immunostaining for 4-HNE adducts of the hearts. (B) Superoxide production of the hearts stained by DHE. Bars = 50 μm. ($n = 5$) (C) Effects of Pyr3 on the expression and activity of Rac1 in MLP (−/−) and MLP (+/+) mouse hearts. n.s.; not significant. ($n = 6$) (D) Average time courses of increase in DCF fluorescence intensity induced by mechanical stretch in rat neonatal cardiomyocytes. Cardiomyocytes were treated with Pyr3 (1 μM) 30 min before mechanical stretch. (E) and (F) Effects of Pyr3 on the OAG-induced ROS production in rat cardiomyocytes. (E) Typical images of DHE accumulation and (F) average increases in DHE fluorescence intensity. Cells were treated with Pyr3 (1 μM) or DPI (1 μM) for 20 min before the addition of OAG (30 μM). Ten min after OAG stimulation, cells were loaded with DHE (2 μM) at 37 °C for 1 h. Bars = 50 μm. ($n = 34–63$) $^{*}P < 0.01$, $^{**}P < 0.001$.

progression of DCM. In the DCM mouse model, the up-regulation of TRPC3 increases not only cardiomyocyte Ca^{2+}-dependent CaMKII activity, but also ROS production. TRPC channels have two functions: to act as receptor-activated or mechanical stretch-activated cation channels in cardiomyocytes, and to act as a protein scaffold at the plasma membrane to control the amplification and co-ordination of receptor signaling [16,33,34]. We previously reported that TRPC3 interacts with phospholipase C and protein kinase C (PKC), leading to sustained activation of an extracellular signal-regulated kinase induced by receptor stimulation in B lymphocytes [33,34]. Activation of PKC contributes to Nox2 activation through phosphorylation of the $p47^{phox}$ subunit [32]. In addition, we found that TRPC3-mediated Ca^{2+} influx also contributes to Rac1 activation in MLP (−/−) mouse hearts (Fig. 4). Although the molecular mechanism underlying activation of Rac1 by Ca^{2+} is still unclear, our results strongly suggest that TRPC3-mediated Ca^{2+} influx controls Nox-dependent ROS production in rodent cardiomyocytes.

Oxidative stress plays a critical role in the progression of DCM, and the major source of ROS production in the heart is mitochondria. Based on the results that the increase in ROS production was associated with an increase in Rac activity in MLP (−/−) mouse hearts, and that the Nox inhibitor suppressed TRPC3-mediated superoxide production in rat cardiomyocytes (Fig. 4), Nox may be a primary source of ROS production. ROS have been reported to induce mitochondrial superoxide production, by a phenomenon reported as ROS-induced ROS release (RIRR) [35,36]. Thus, TRPC3-mediated Ca^{2+} influx in rodent cardiomyocytes may initially induce Nox-dependent ROS production, with the subsequent induction of an oxygen burst through RIRR-mediated ROS production.

Previous reports have shown that ablation of AT_1R or expression of βARK-ct attenuates LV dysfunction in MLP (−/−) mice. We also reported that TRPC3/TRPC6 mediates Ang II-induced cardiomyocyte hypertrophy [21], suggesting that AT_1R works upstream of TRPC3 in MLP (−/−) mouse hearts. In contrast, βARK-ct inhibits βARK1-mediated β_1AR internalization through sequestration of the βγ subunit (Gβγ) released from the α_s subunit of G proteins coupled to β_1AR. However, inhibition of TRPC3 does not affect β_1AR-mediated Ca^{2+} signaling in rat cardiomyocytes (unpublished data). As βARK is activated by Gαq-mediated PKC activation in rat cardiomyocytes [37], one explanation is that TRPC3 contributes to PKC-mediated βARK activation downstream of AT_1R signaling in the heart [34].

Both Ca^{2+}/calmodulin-dependent calcineurin and CaMKII function as key mediators in the development of cardiac hypertrophy [38,39]. Cardiomyocyte-specific overexpression of the constitutively active mutant of NFAT causes cardiac hypertrophy, whereas expression of calcineurin or CaMKII causes cardiomyopathy [13,40]. Although calcineurin/NFAT signaling may participate in the development of hypertrophy, CaMKII may participate in the development of heart failure. Since the inhibition of TRPC3 suppresses both calcineurin/NFAT and CaMKII signaling pathways in cardiomyocytes, our findings strongly suggest TRPC3 channels as a putative therapeutic target for the treatment of heart failure.

Acknowledgments

This study was supported by grants from Grant-in-Aid for Scientific Research on Innovative Areas (M. Nishida); from the Ministry of Education, Culture, Sports, Science, and Technology of Japan (to M. Nishida, M. Nakaya and H. Kurose); from the Institute of Seizon and Life Sciences (to S. Morimoto) and from Naito Foundation and Mochida Memorial Foundation (M. Nishida). M. Hoshijima was supported by NIH (R01 HL081401) and American Heart Association (0840013N).

References

[1] J.A. Towbin, A.M. Lowe, S.D. Colan, et al., Incidence, causes, and outcomes of dilated cardiomyopathy in children, JAMA 296 (2006) 1867–1876.
[2] W.B. Maclellan, A. Lusis, Dilated cardiomyopathy: learning to live with yourself, Nat. Med. 9 (2003) 1455–1456.
[3] E. Grunig, J.A. Tasman, H. Kucherer, et al., Frequency and phenotypes of familial dilated cardiomyopathy, J. Am. Coll. Cardiol. 31 (1998) 186–194.
[4] J.A. Towbin, N.E. Bowles, The failing heart, Nat. Insight rev. articles 415 (2002) 227–233.
[5] C.-K. Du, S. Morimoto, K. Nishii, et al., Knock-in model of dilated cardiomyopathy caused by troponin mutation, Circ. Res. 101 (2007) 185–194.
[6] S. Arber, G. Halder, P. Caroni, Muscle LIM protein, a novel essential regulator of myogenesis, promotes myogenic differentiation, Cell 79 (1994) 221–231.
[7] S. Arber, J.J. Hunter, J. Ross Jr, et al., MLP-deficient mice exhibit a disruption of cardiac cytoarchitectural organization, dilated cardiomyopathy, and heart failure, Cell 88 (1997) 393–403.
[8] R. Knöll, M. Hoshijima, H.M. Hoffman, et al., The cardiac mechanical stretch sensor machinery involves a Z-disc complex that is defective in a subset of human dilated cardiomyopathy, Cell 111 (2002) 943–955.
[9] R. Knöll, S. Kostin, S. Klede, et al., A common MLP (muscle LIM protein) variant is associated with cardiomyopathy, Circ. Res. 106 (2010) 695–704.
[10] R. Yamamoto, H. Akazawa, K. Ito, et al., Angiotensin II type 1a receptor signals are involved in the progression of heart failure in MLP-deficient mice, Circ. J. 71 (2007) 1958–1964.
[11] H.A. Rockman, K.R. Chien, D.-J. Choi, et al., Expression of a β-adrenergic receptor kinase 1 inhibitor prevents the development of myocardial failure in gene-targeted mice, Proc. Natl. Acad. Sci. USA 95 (1998) 7000–7005.
[12] X. Wang, V.C. Culotta, C.B. Klee, Superoxide dismutase protects calcineurin from inactivation, Nature 383 (1996) 434–437.
[13] H. Toko, H. Takahashi, Y. Kayama, et al., Ca^{2+}/calmodulin-dependent kinase IIδ causes heart failure by accumulation of p53 in dilated cardiomyopathy, Circulation 122 (2010) 891–899.
[14] C. Maack, T. Kartes, H. Kilter, et al., Oxygen free radical release in human failing myocardium is associated with increased activity of Rac1-GTPase and represents a target for statin treatment, Circulation 108 (2003) 1567–1574.
[15] C. Montell, G.M. Rubin, Molecular characterization of the Drosophila trp locus: a putative integral membrane protein required for phototransduction, Neuron 2 (1989) 1313–1323.
[16] M. Nishida, Y. Hara, T. Yoshida, et al., TRP channels: molecular diversity and physiological function, Microcirculation 13 (2006) 535–550.
[17] M. Nishida, H. Kurose, Roles of TRP channels in the development of cardiac hypertrophy, Naunyn–Schmiedeberg's Arch. Pharmacol. 378 (2008) 395–406.
[18] E.W. Bush, D.B. Hood, P.J. Papst, et al., Canonical transient receptor potential channels promote cardiomyocyte hypertrophy through activation of calcineurin signaling, J. Biol. Chem. 281 (2006) 33487–33496.
[19] K. Kuwahara, Y. Wang, J. McAnally, et al., TRPC6 fulfills a calcineurin signaling circuit during pathologic cardiac remodeling, J. Clin. Invest. 116 (2006) 3114–3126.
[20] M. Seth, Z.S. Zhang, L. Mao, et al., TRPC1 channels are critical for hypertrophic signaling in the heart, Circ. Res. 105 (2009) 1023–1030.
[21] N. Onohara, M. Nishida, R. Inoue, et al., TRPC3 and TRPC6 are essential for angiotensin II-induced cardiac hypertrophy, EMBO J. 25 (2006) 5305–5316.
[22] S. Kiyonaka, K. Kato, M. Nishida, et al., Selective and direct inhibition of TRPC3 channels underlies biological activities of a pyrazole compound, Proc. Natl. Acad. Sci. USA 106 (2009) 5400–5405.
[23] J. Heineke, H. Ruetten, C. Willenbockel, et al., Attenuation of cardiac remodeling after myocardial infarction by muscle LIM protein-calcineurin signaling at the sarcomeric Z-disc, Proc. Natl. Acad. Sci. USA 102 (2005) 1655–1660.
[24] M. Nishida, Y. Sato, A. Uemura, et al., $P2Y_6$ receptor-$G\alpha 12_{/13}$ signalling in cardiomyocytes triggers pressure overload-induced cardiac fibrosis, EMBO J. 27 (2008) 3104–3115.
[25] M. Nishida, Y. Maruyama, R. Tanaka, et al., Gαi and Gαo are target proteins of reactive oxygen species, Nature 408 (2000) 492–495.
[26] M. Nishida, K. Watanabe, Y. Sato, et al., Phosphorylation of TRPC6 channels at Thr69 is required for anti-hypertrophic effects of phosphodiesterase 5 inhibition, J. Biol. Chem. 285 (2010) 13244–13253.
[27] T. Fujii, N. Onohara, Y. Maruyama, et al., $G\alpha 12_{/13}$-mediated production of reactive oxygen species is critical for angiotensin receptor-induced NFAT activation in cardiac fibroblasts, J. Biol. Chem. 280 (2005) 23041–23047.
[28] D. Granfeldt, M. Samuelsson, A. Karlsson, Capacitative Ca^{2+} influx and activation of the neutrophil respiratory burst. Different regulation of plasma membrane-and granule-localized NADPH-oxidase, J. Leukoc. Biol. 71 (2002) 611–617.
[29] D.B. Graham, C.M. Robertson, J. Bautista, et al., Neutrophil-mediated oxidative burst and host defense are controlled by a Vav-PLCγ2 signaling axis in mice, J. Clin. Invest. 117 (2007) 3445–3452.
[30] J.M. Li, N.P. Gall, D.J. Grieve, et al., Activation of NADPH oxidase during progression of cardiac hypertrophy to failure, Hypertension 40 (2002) 477–484.
[31] T. Ago, J. Kuroda, J. Pain, et al., Upregulation of Nox4 by hypertrophic stimuli promotes apoptosis and mitochondrial dysfunction in cardiac myocytes, Circ. Res. 106 (2010) 1253–1264.
[32] H. Sumimoto, Structure, regulation and evolution of Nox-family NADPH oxidases that produce reactive oxygen species, FEBS J. 275 (2008) 3249–3277.
[33] M. Nishida, K. Sugimoto, Y. Hara, et al., Amplification of receptor signaling by Ca^{2+} entry-mediated translocation and activation of PLCγ2 in B lymphocytes, EMBO J. 22 (2003) 4677–4688.
[34] T. Numaga, M. Nishida, S. Kiyonaka, et al., Ca^{2+} influx and protein scaffolding via TRPC3 sustain PKCβ and ERK activation in B cells, J. Cell. Sci. 123 (2010) 927–938.
[35] D.B. Zorov, C.R. Filburn, L.O. Klotz, et al., Reactive oxygen species (ROS)-induced ROS release: a new phenomenon accompanying induction of the mitochondrial permeability transition in cardiac myocytes, J. Exp. Med. 192 (2000) 1001–1014.
[36] N.R. Brady, A. Hamacher-Brady, H.V. Westerhoff, et al., A wave of reactive oxygen species (ROS)-induced ROS release in a sea of excitable mitochondria, Antioxid. Redox. Signal. 8 (2006) 1651–1665.
[37] R. Malhotra, K.M. D'Souza, M.L. Staron, et al., Gαq-mediated activation of GRK2 by mechanical stretch in cardiac myocytes: the role of protein kinase C, J. Biol. Chem. 285 (2010) 13748–13760.
[38] J.D. Molkentin, J.-R. Lu, C.L. Antos, et al., A calcineurin-dependent transcriptional pathway for cardiac hypertrophy, Cell 93 (1998) 215–228.
[39] R. Passier, H. Zeng, N. Frey, et al., CaM kinase signaling induces cardiac hypertrophy and activates the MEF2 transcription factor *in vivo*, J. Clin. Invest. 105 (2000) 1395–1406.
[40] M.R. Sayen, A.B. Gustafsson, M.A. Sussman, et al., Calcineurin transgenic mice have mitochondrial dysfunction and elevated superoxide production, Am. J. Physiol. Cell Physiol. 284 (2003) C562–570.

Efficient Generation of Functional Hepatocytes From Human Embryonic Stem Cells and Induced Pluripotent Stem Cells by HNF4α Transduction

Kazuo Takayama[1,2], Mitsuru Inamura[1,2], Kenji Kawabata[2,3], Kazufumi Katayama[1], Maiko Higuchi[2], Katsuhisa Tashiro[2], Aki Nonaka[2], Fuminori Sakurai[1], Takao Hayakawa[4,5], Miho Kusuda Furue[6,7] and Hiroyuki Mizuguchi[1,2,8]

[1]Laboratory of Biochemistry and Molecular Biology, Graduate School of Pharmaceutical Sciences, Osaka University, Osaka, Japan; [2]Laboratory of Stem Cell Regulation, National Institute of Biomedical Innovation, Osaka, Japan; [3]Laboratory of Biomedical Innovation, Graduate School of Pharmaceutical Sciences, Osaka University, Osaka, Japan; [4]Pharmaceutics and Medical Devices Agency, Tokyo, Japan; [5]Pharmaceutical Research and Technology Institute, Kinki University, Osaka, Japan; [6]JCRB Cell Bank, Division of Bioresources, National Institute of Biomedical Innovation, Osaka, Japan; [7]Laboratory of Cell Processing, Institute for Frontier Medical Sciences, Kyoto University, Kyoto, Japan; [8]The Center for Advanced Medical Engineering and Informatics, Osaka University, Osaka, Japan

Hepatocyte-like cells from human embryonic stem cells (ESCs) and induced pluripotent stem cells (iPSCs) are expected to be a useful source of cells drug discovery. Although we recently reported that hepatic commitment is promoted by transduction of SOX17 and HEX into human ESC- and iPSC-derived cells, these hepatocyte-like cells were not sufficiently mature for drug screening. To promote hepatic maturation, we utilized transduction of the hepatocyte nuclear factor 4α (HNF4α) gene, which is known as a master regulator of liver-specific gene expression. Adenovirus vector-mediated overexpression of HNF4α in hepatoblasts induced by SOX17 and HEX transduction led to upregulation of epithelial and mature hepatic markers such as cytochrome P450 (CYP) enzymes, and promoted hepatic maturation by activating the mesenchymal-to-epithelial transition (MET). Thus HNF4α might play an important role in the hepatic differentiation from human ESC-derived hepatoblasts by activating the MET. Furthermore, the hepatocyte like-cells could catalyze the toxication of several compounds. Our method would be a valuable tool for the efficient generation of functional hepatocytes derived from human ESCs and iPSCs, and the hepatocyte-like cells could be used for predicting drug toxicity.

Received 19 July 2011; accepted 28 September 2011; published online 8 November 2011. doi:10.1038/mt.2011.234

INTRODUCTION

Human embryonic stem cells (ESCs) and induced pluripotent stem cells (iPSCs) are able to replicate indefinitely and differentiate into most of the body's cell types.[1,2] They could provide an unlimited source of cells for various applications. Hepatocyte-like cells, which are differentiated from human ESCs and iPSCs, would be useful for basic research, regenerative medicine, and drug discovery.[3] In particular, it is expected that hepatocyte-like cells will be utilized as a tool for cytotoxicity screening in the early phase of pharmaceutical development. To catalyze the toxication of several compounds, hepatocyte-like cells need to be mature enough to exhibit hepatic functions, including high activity levels of the cytochrome P450 (CYP) enzymes. Because the present technology for the generation of hepatocyte-like cells from human ESCs and iPSCs, which is expected to be utilized for drug discovery, is not refined enough for this application, it is necessary to improve the efficiency of hepatic differentiation. Although conventional methods such as growth factor-mediated hepatic differentiation are useful to recapitulate liver development, they lead to only a heterogeneous hepatocyte population.[4–6] Recently, we showed that transcription factors are transiently transduced to promote hepatic differentiation in addition to the conventional differentiation method which uses only growth factors.[7] Ectopic expression of Sry-related HMG box 17 (SOX17) or hematopoietically expressed homeobox (HEX) by adenovirus (Ad) vectors in human ESC-derived mesendoderm or definitive endoderm (DE) cells markedly enhances the endoderm differentiation or hepatic commitment, respectively.[7,8] However, further hepatic maturation is required for drug screening.

The transcription factor hepatocyte nuclear factor 4α (HNF4α) is initially expressed in the developing hepatic diverticulum on E8.75,[9,10] and its expression is elevated as the liver develops. A previous loss-of-function study showed that HNF4α plays a critical role in liver development; conditional deletion of *HNF4α* in fetal hepatocytes results in the faint expression of many mature hepatic enzymes and the impairment of normal liver morphology.[11] The genome-scale chromatin immunoprecipitation assay showed that HNF4α binds to the promoters of nearly half of the genes expressed in the mouse liver,[12] including cell adhesion and junctional proteins,[13] which are important in

Correspondence: Hiroyuki Mizuguchi, Laboratory of Biochemistry and Molecular Biology, Graduate School of Pharmaceutical Sciences, Osaka University, 1-6 Yamadaoka, Suita, Osaka 565-0871, Japan. E-mail: mizuguch@phs.osaka-u.ac.jp

the hepatocyte epithelial structure.[14] In addition, HNF4α plays a critical role in hepatic differentiation and in a wide variety of liver functions, including lipid and glucose metabolism.[15,16] Although HNF4α could promote transdifferentiation into hepatic lineage from hematopoietic cells,[17] the function of HNF4α in hepatic differentiation from human ESCs and iPSCs remains unknown. A previous study showed that hepatic differentiation from mouse hepatic progenitor cells is promoted by HNF4α, although many of the hepatic markers that they examined were target genes of HNF4α.[18] They transplanted the HNF4α-overexpressed mouse hepatic progenitor cells to promote hepatic differentiation, but they did not examine the markers that relate to hepatic maturation such as CYP enzymes, conjugating enzymes, and hepatic transporters.

In this study, we examined the role of HNF4α in hepatic differentiation from human ESCs and iPSCs. The human ESC- and iPSC-derived hepatoblasts, which were efficiently generated by sequential transduction of SOX17 and HEX, were transduced with HNF4α-expressing Ad vector (Ad-HNF4α), and then the expression of hepatic markers of the hepatocyte-like cells were assessed. In addition, we examined whether or not the hepatocyte-like cells, which were generated by sequential transduction of SOX17, HEX, and HNF4α, were able to predict the toxicity of several compounds.

RESULTS

Stage-specific HNF4α transduction in hepatoblasts selectively promotes hepatic differentiation

The transcription factor HNF4α plays an important role in both liver generation[11] and hepatic differentiation from human ESCs and iPSCs (**Supplementary Figure S1**). We expected that hepatic differentiation could be accelerated by HNF4α transduction. To examine the effect of forced expression of HNF4α in the hepatic differentiation from human ESC- and iPSC-derived cells, we used a fiber-modified Ad vector.[19] Initially, we optimized the time period for Ad-HNF4α transduction. Human ESC (H9)-derived DE cells (day 6) (**Supplementary Figures S2** and **S3a**), hepatoblasts (day 9) (**Supplementary Figures S2** and **S3b**), or a heterogeneous population consisting of hepatoblasts, hepatocytes, and cholangiocytes (day 12) (**Supplementary Figures S2** and **S3c**) were transduced with Ad-HNF4α and then the Ad-HNF4α-transduced cells were cultured until day 20 of differentiation (**Figure 1**). We ascertained the expression of exogenous *HNF4α* in human ESC-derived hepatoblasts (day 9) transduced with Ad-HNF4α (**Supplementary Figure S4**). The transduction of Ad-HNF4α into human ESC-derived hepatoblasts (day 9) led to the highest expression levels of the hepatocyte markers *albumin* (*ALB*)[20] and *α-1-antitrypsin* (**Figure 1a**). In contrast, the expression levels of the cholangiocyte markers *cytokeratin 7* (*CK7*)[21] and *SOX9*[22] were

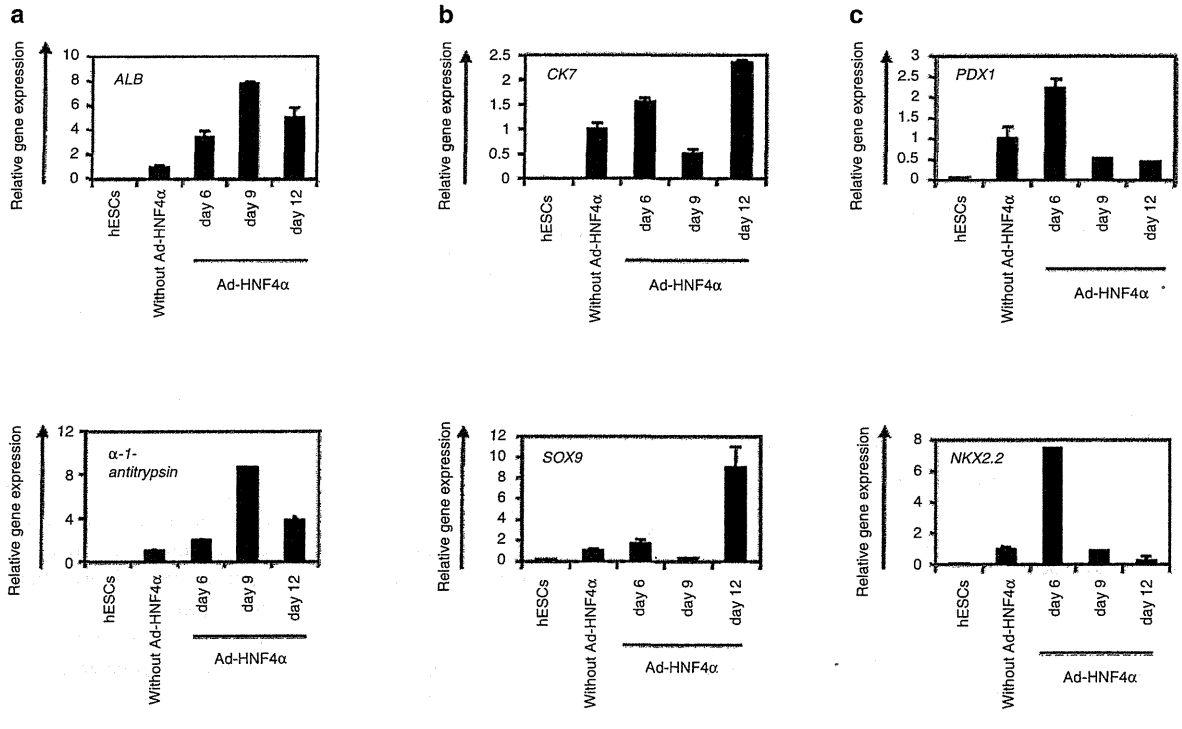

Figure 1 Transduction of HNF4α into hepatoblasts promotes hepatic differentiation. (**a–c**) The human ESC (H9)-derived cells, which were cultured for 6, 9, or 12 days according to the protocol described in **Figure 2a**, were transduced with 3,000 vector particles (VP)/cell of Ad-HNF4α for 1.5 hours and cultured until day 20. The gene expression levels of (**a**) hepatocyte markers (*ALB* and *α-1-antitrypsin*), (**b**) cholangiocyte markers (*CK7* and *SOX9*), and (**c**) pancreas markers (*PDX1* and *NKX2.2*) were examined by real-time RT-PCR on day 0 (human ESCs (hESCs)) or day 20 of differentiation. The horizontal axis represents the days when the cells were transduced with Ad-HNF4α. On the y-axis, the level of the cells without Ad-HNF4α transduction on day 20 was taken as 1.0. All data are represented as means ± SD ($n = 3$). ESC, embryonic stem cell; HNF4α, hepatocyte nuclear factor 4α; RT-PCR, reverse transcription-PCR.

downregulated in the cells transduced on day 9 as compared with nontransduced cells (**Figure 1b**). This might be because hepatic differentiation was selectively promoted and biliary differentiation was repressed by the transduction of HNF4α in hepatoblasts. The expression levels of the pancreas markers *PDX1*[23] and *NKX2.2*[24] did not make any change in the cells transduced on day 9 as compared with nontransduced cells (**Figure 1c**). Interestingly, the expression levels of the pancreas markers were upregulated, when Ad-HNF4α transduction was performed into DE cells (day 6) (**Figure 1c**). These results suggest that HNF4α might promote not only hepatic differentiation but also pancreatic differentiation, although the optimal stage of HNF4 transduction for the differentiation of each cell is different. We have confirmed that there was no difference between nontransduced cells and Ad-LacZ-transduced cells in the gene expression levels of all the markers investigated in **Figure 1a–c** (data not shown). We also confirmed that Ad vector-mediated gene expression in the human ESC-derived hepatoblasts (day 9) continued until day 14 and almost disappeared on day 18 (**Supplementary Figure S5**). These results indicated that the stage-specific HNF4α overexpression in human ESC-derived hepatoblasts (day 9) was essential for promoting efficient hepatic differentiation.

Transduction of HNF4α into human ESC- and iPSC-derived hepatoblasts efficiently promotes hepatic maturation

From the results of **Figure 1**, we decided to transduce hepatoblasts (day 9) with Ad-HNF4α. To determine whether hepatic maturation is promoted by Ad-HNF4α transduction, Ad-HNF4α-transduced cells were cultured until day 20 of differentiation according to the schematic protocol described in **Figure 2a**. After the hepatic maturation, the morphology of human ESCs was gradually changed into that of hepatocytes: polygonal with distinct round nuclei (day 20) (**Figure 2b**). Interestingly, a portion of the hepatocyte-like cells, which were ALB[20]-, CK18[21]-, CYP2D6-, and CYP3A4[25]-positive cells, had double nuclei, which was also observed in primary human hepatocytes (**Figure 2b,c**, and **Supplementary Figure S6**). We also examined the hepatic gene expression levels on day 20 of differentiation (**Figure 3a,b**). The gene expression analysis of *CYP1A2*, *CYP2C9*, *CYP2C19*, *CYP2D6*, *CYP3A4*, and *CYP7A1*[25] showed higher expression levels in all of Ad-SOX17-, Ad-HEX-, and Ad-HNF4α-transduced cells (three factors-transduced cells) as compared with those in both Ad-SOX17- and Ad-HEX-transduced cells (two factors-transduced cells) on day 20 (**Figure 3a**). The gene expression level of NADPH-CYP reductase

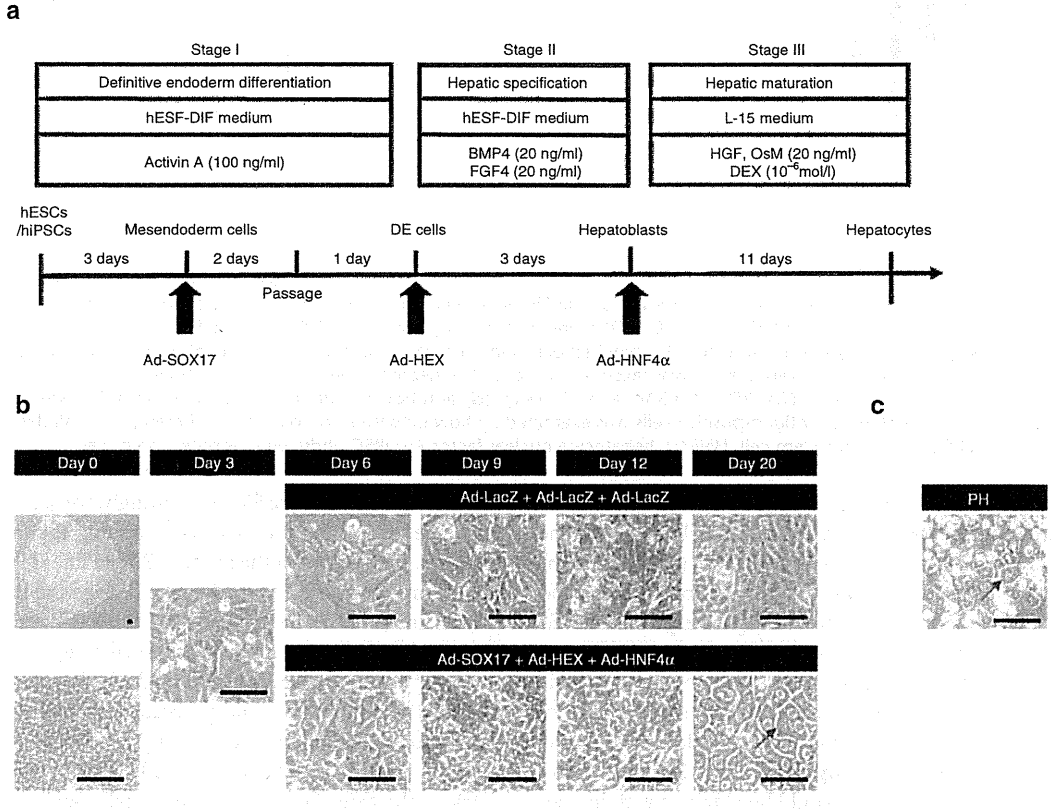

Figure 2 Hepatic differentiation of human ESCs and iPSCs transduced with three factors. (**a**) The procedure for differentiation of human ESCs and iPSCs into hepatocytes via DE cells and hepatoblasts is presented schematically. The hESF-DIF medium was supplemented with 10 μg/ml human recombinant insulin, 5 μg/ml human apotransferrin, 10 μmol/l 2-mercaptoethanol, 10 μmol/l ethanolamine, 10 μmol/l sodium selenite, and 0.5 mg/ml fatty-acid-free BSA. The L15 medium was supplemented with 8.3% tryptose phosphate broth, 8.3% FBS, 10 μmol/l hydrocortisone 21-hemisuccinate, 1 μmol/l insulin, and 25 mmol/l $NaHCO_3$. (**b**) Sequential morphological changes (day 0–20) of human ESCs (H9) differentiated into hepatocytes via DE cells and hepatoblasts are shown. Red arrow shows the cells that have double nuclei. (**c**) The morphology of primary human hepatocytes is shown. Bar represents 50 μm. BSA, bovine serum albumin; DE, definitive endoderm; ESC, embryonic stem cell; iPSC, induced pluripotent stem cell.

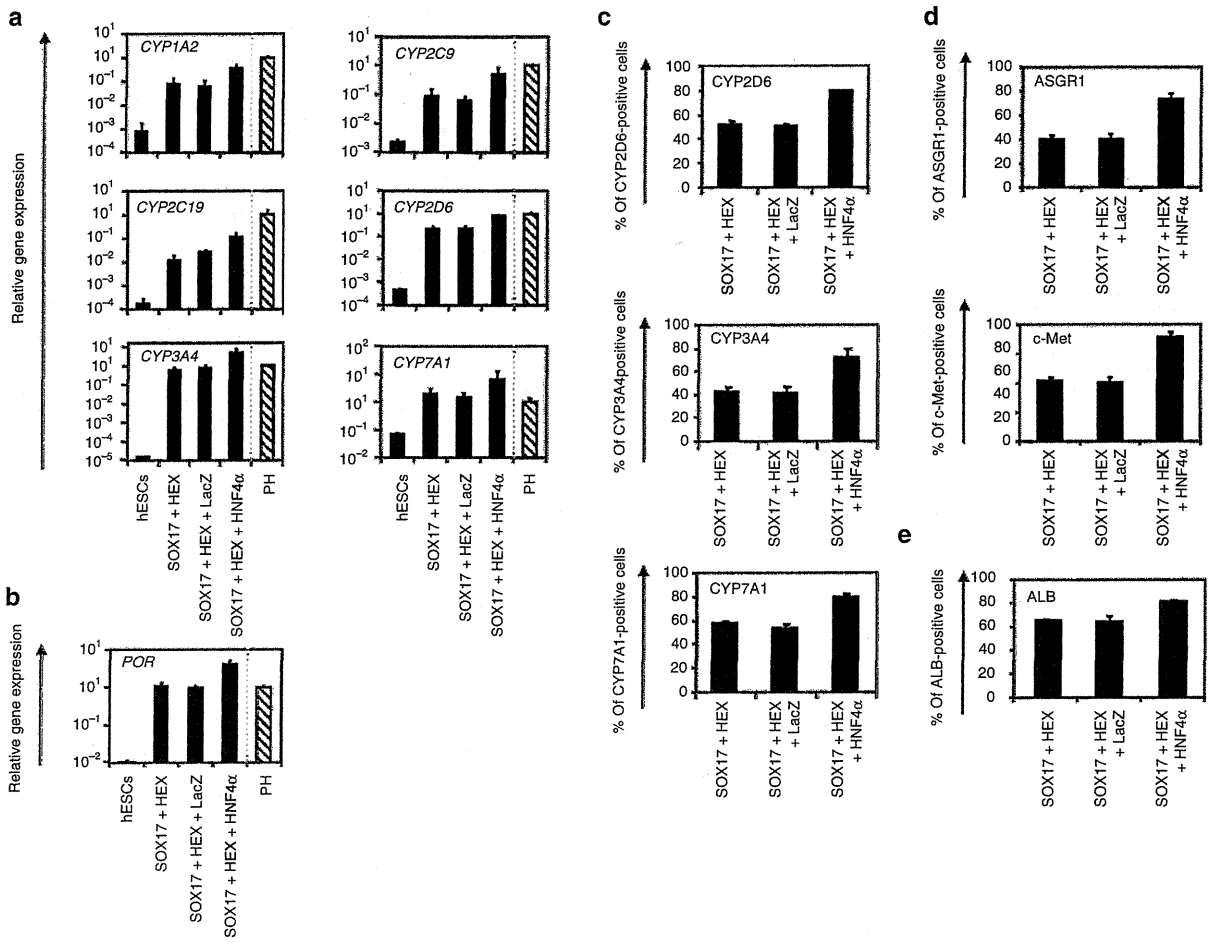

Figure 3 Transduction of HNF4α promotes hepatic maturation from human ESCs and iPSCs. (**a**,**b**) The human ESCs were differentiated into hepatocytes according to the protocol described in **Figure 2a**. On day 20 of differentiation, the gene expression levels of (**a**) CYP enzymes (*CYP1A2, CYP2C9, CYP2C19, CYP2D6, CYP3A4,* and *CYP7A1*) and (**b**) *POR* were examined by real-time RT-PCR in undifferentiated human ESCs (hESCs), the hepatocyte-like cells, and primary human hepatocytes (PH, hatched bar). On the y-axis, the expression level of primary human hepatocytes, which were cultured for 48 hours after the cells were plated, was taken as 1.0. (**c**–**e**) The hepatocyte-like cells (day 20) were subjected to immunostaining with (**c**) anti-drug-metabolizing enzymes (CYP2D6, CYP3A4, and CYP7A1), (**d**) anti-hepatic surface protein (ASGR1 and c-Met), and (**e**) anti-ALB antibodies, and then the percentage of antigen-positive cells was examined by flow cytometry on day 20 of differentiation. All data are represented as means ± SD (n = 3). ESC, embryonic stem cell; HNF4α, hepatocyte nuclear factor 4α; iPSC, induced pluripotent stem cell.

(POR)[26], which is required for the normal function of CYPs, was also higher in the three factors-transduced cells (**Figure 3b**). The gene expression analysis of ALB, α-1-antitrypsin (α-1-AT), transthyretin, hepatic conjugating enzymes, hepatic transporters, and hepatic transcription factors also showed higher expression levels in the three factors-transduced cells (**Supplementary Figures S7** and **S8**). Moreover, the gene expression levels of these hepatic markers of three factor-transduced cells were similar to those of primary human hepatocytes, although the levels depended on the type of gene (**Figure 3a,b**, and **Supplementary Figures S7** and **S8**). To confirm that similar results could be obtained with human iPSCs, we used three human iPS cell lines (201B7, Dotcom, and Tic). The gene expression of hepatic markers in human ESC- and iPSC-derived hepatocytes were analyzed by real-time reverse transcription-PCR on day 20 of differentiation. Three human iPS cell lines as well as human ESCs also effectively differentiated into hepatocytes in response to transduction of the three factors (**Supplementary Figure S9**). Interestingly, we observed differences in the hepatic maturation efficiency among the three human iPS cell lines. That is, two of the human iPS cell lines (Tic and Dotcom) were more committed to the hepatic lineage than another human iPS cell line (201B7). Because almost homogeneous hepatocyte-like cells would be more useful in basic research, regenerative medicine, and drug discovery, we also examined whether our novel methods for hepatic maturation could generate a homogeneous hepatocyte population by flow cytometry analysis (**Figure 3c–e**). The percentages of CYP2D6-, CYP3A4-, and CYP7A1-positive cells were ~80% in the three factors-transduced cells, while they were ~50% in the two factors-transduced cells (**Figure 3c**). The percentages of hepatic surface antigen (asialoglycoprotein receptor 1 (ASGR1] and met proto-oncogene (c-Met))-positive cells (**Figure 3d**) and ALB-positive cells (**Figure 3e**) were also ~80% in the three factors-transduced cells. These results indicated that a nearly homogeneous population was obtained by our differentiation protocol

using the transduction of three functional genes (SOX17, HEX, and HNF4α).

The three factors-transduced cells have characteristics of functional hepatocytes

The hepatic functions of the hepatocyte-like cells, such as the uptake of low-density lipoprotein (LDL) and CYP enzymes activity, of the hepatocyte-like cells were examined on day 20 of differentiation. Approximately 87% of the three factors-transduced cells uptook LDL in the medium, whereas only 44% of the two factors-transduced cells did so (**Figure 4a**). The activities of CYP enzymes of the hepatocyte-like cells were measured according to the metabolism of the CYP3A4, CYP2C9, or CYP1A2 substrates (**Figure 4b**). The metabolites were detected in the three factors-transduced cells and their activities were higher than those of the two factors-transduced cells (dimethyl sulfoxide (DMSO) column). We further tested the induction of CYP3A4, CYP2C9, and CYP1A2 by chemical stimulation, since CYP3A4, CYP2C9, and CYP1A2 are the important prevalent CYP isozymes in the liver and are involved in the metabolism of a significant proportion of the currently available commercial drugs (rifampicin or omeprazole column). It is well known that CYP3A4 and CYP2C9 can be induced by rifampicin, whereas CYP1A2 can be induced by omeprazole. The hepatocyte-like cells were treated with either of these. Although undifferentiated human ESCs responsed to neither rifampicin nor omeprazole (data not shown), the hepatocyte-like cells produced more metabolites in response to chemical stimulation as well as primary hepatocytes (**Figure 4b**). The activity levels of the hepatocyte-like cells as compared with those of primary human hepatocytes depended on the types of CYP; the CYP3A4 activity of the hepatocyte-like cells was similar to that of primary human hepatocytes, whereas the CYP2C9 and CYP1A2 activities of the hepatocyte-like cells were slightly lower than those of primary human hepatocytes (**Figure 3a**). These results indicated that high levels of functional CYP enzymes were detectable in the hepatocyte-like cells.

The metabolism of diverse compounds involving uptake, conjugation, and the subsequent release of the compounds is an important function of hepatocytes. Uptake and release of Indocyanine green (ICG) can often be used to identify hepatocytes in ESC differentiation models.[27] To investigate this function in our hepatocyte-like cells, we compared this ability of the three factors-transduced cells with that of the two factors-transduced cells on day 20 of differentiation (**Figure 4c**). The three factors-transduced cells had more ability to uptake ICG and to excrete ICG by culturing without ICG for 6 hours. We also examined whether the hepatocyte-like cells could store glycogen, a characteristic of functional hepatocytes (**Figure 4d**). On day 20 of differentiation, the three factors-transduced cells and the two factors-transduced cells were stained for cytoplasmic glycogen using the Periodic Acid-Schiff staining procedure. The three factors-transduced cells exhibited more abundant storage of glycogen than the two-factors-transduced cells. These results showed that abundant hepatic functions, such as uptake and excretion of ICG and storage of glycogen, were obtained by the transduction of three factors.

Many adverse drug reactions are caused by the CYP-dependent activation of drugs into reactive metabolites.[28] In order to examine metabolism-mediated toxicity and to improve the safety of drug candidates, primary human hepatocytes are widely used.[28] Because primary human hepatocytes have quite different characteristics among distinct lots and because it is difficult to purchase large amounts of primary human hepatocytes that have the same characteristics, hepatocyte-like cells are expected to be used for this purpose. To examine whether our hepatocyte-like cells could be used to predict metabolism-mediated toxicity, the hepatocyte-like cells were incubated with four substrates (troglitazone, acetaminophen, cyclophosphamide, and carbamazepine), which are known to generate toxic metabolites by CYP enzymes, and then the cell viability was measured (**Figure 4e**). The cell viability of the two factors plus Ad-LacZ-tansduced cells were higher than that of the three factors-transduced cells at each different concentration of four test compounds. These results indicated that the three factors-transduced cells could more efficiently metabolize the test compounds and thereby induce higher toxicity than either the two factors-transduced cells or undifferentiated human ESCs. The cell viability of the three factors-transduced cells was slightly higher than that of primary human hepatocytes.

HNF4α promotes hepatic maturation by activating mesenchymal-to-epithelial transition

HNF4α is known as a dominant regulator of the epithelial phenotype because its ectopic expression in fibroblasts (such as NIH 3T3 cells) induces mesenchymal-to-epithelial transition (MET)[11], although it is not known whether HNF4α can promote MET in hepatic differentiation. Therefore, we examined whether HNF4α transduction promotes hepatic maturation from hepatoblasts by activating MET. To clarify whether MET is activated by HNF4α transduction, the human ESC-derived hepatoblasts (day 9) were transduced with Ad-LacZ or Ad-HNF4α, and the resulting phenotype was analyzed on day 12 of differentiation (**Figure 5**). This time, we confirmed that HNF4α transduction decreased the population of N-cadherin (hepatoblast marker)-positive cells,[29] whereas it increased that of ALB (hepatocyte marker)-positive cells (**Figure 5a**). The number of CK7 (cholangiocyte marker)-positive population did not change (**Figure 5a**). To investigate whether these results were attributable to MET, the alteration of the expression of several mesenchymal and epithelial markers was examined (**Figure 5b**). The human ESC-derived hepatoblasts (day 9) were almost homogeneously N-cadherin[30] (mesenchymal marker)-positive and E-cadherin[11] (epithelial marker)-negative, demonstrating that human ESC-derived hepatoblasts have mesenchymal characteristics (**Figure 5a,b**). After HNF4α transduction, the number of E-cadherin-positive cells was increased and reached ~90% on day 20, whereas that of N-cadherin-positive cells was decreased and was less than 5% on day 20 (**Supplementary Figure S10**). These results indicated that MET was promoted by HNF4α transduction in hepatic differentiation from hepatoblasts. Interestingly, the number of growing cells was decreased by HNF4α transduction (**Figure 5c**), and the cell growth was delayed by HNF4α transduction (**Supplementary Figure S11**). This decrease in the number of growing cells might have been because the differentiation was promoted by HNF4α transduction. We also confirmed that MET was promoted by HNF4α transduction in the gene expression levels (**Figure 5d**).

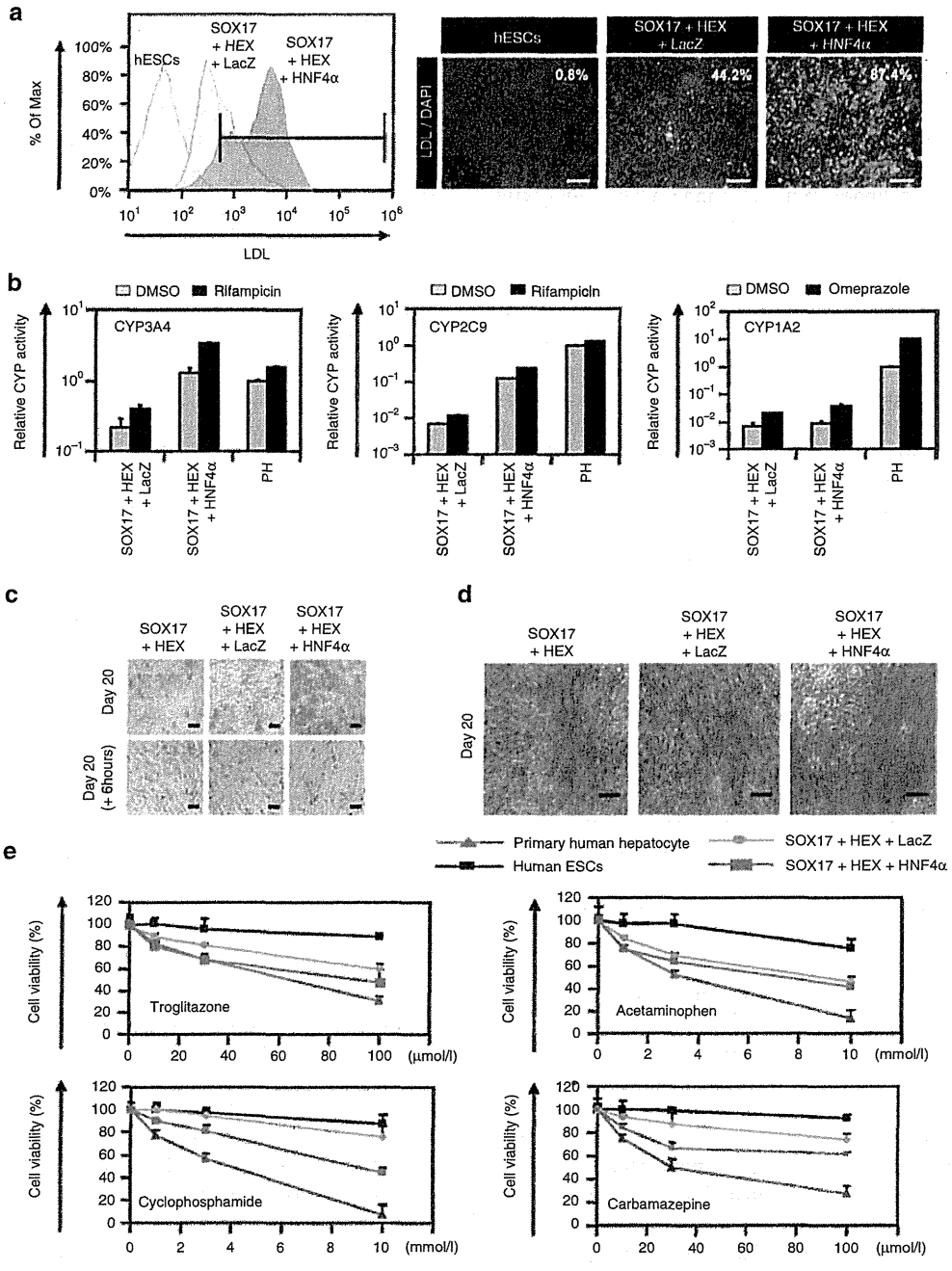

Figure 4 Transduction of the three factors enhances hepatic functions. The human ESCs were differentiated into hepatoblasts and transduced with 3,000 VP/cell of Ad-LacZ or Ad-HNF4α for 1.5 hours and cultured until day 20 of differentiation according to the protocol described in **Figure 2a**. The hepatic functions of the two factors plus Ad-LacZ-transduced cells (SOX17+HEX+LacZ) and the three factors-transduced cells (SOX17+HEX+HNF4α) were compared. (**a**) Undifferentiated human ESCs (hESCs) and the hepatocyte-like cells (day 20) were cultured with medium containing Alexa-Flour 488-labeled LDL (green) for 1 hour, and immunohistochemistry and flow cytometry analysis were performed. The percentage of LDL-positive cells was measured by flow cytometry. Nuclei were counterstained with DAPI (blue). The bar represents 100 μm. (**b**) Induction of CYP3A4 (left), CYP2C9 (middle), or CYP1A2 (right) by DMSO (gray bar), rifampicin (black bar), or omeprazole (black bar) in the hepatocyte-like cells (day 20) and primary human hepatocytes (PH), which were cultured for 48 hours after the cells were plated. On the y-axis, the activity of primary human hepatocytes that have been cultured with medium containing DMSO was taken as 1.0. (**c**) The hepatocyte-like cells (day 20) (upper column) were examined for their ability to take up Indocyanin Green (ICG) and release it 6 hours thereafter (lower column). (**d**) Glycogen storage of the hepatocyte-like cells (day 20) was assessed by Periodic Acid-Schiff (PAS) staining. PAS staining was performed on day 20 of differentiation. Glycogen storage is indicated by pink or dark red-purple cytoplasms. The bar represents 100 μm. (**e**) The cell viability of undifferentiated human ESCs (black), two factors plus Ad-LacZ-tansduced cells (green), the three factors-transduced cells (blue), and primary human hepatocytes (red) was assessed by Alamar Blue assay after 48 hours exposure to different concentrations of four test compounds (troglitazone, acetaminophen, cyclophosphamide, and carbamazepine). The cell viability is expressed as a percentage of cells treated with solvent only treat: 0.1% DMSO except for carbamazepine: 0.5% DMSO. All data are represented as means ± SD (n = 3). ESC, embryonic stem cell; DMSO, dimethyl sulfoxide; LDL, low-density lipoprotein.